ARTICLES
https://doi.org/10.1038/s41593-021-00927-0
nature neuroscience

Check for updates

Genetically identified amygdala–striatal circuits for valence-specific behaviors

Xian Zhang[1]✉, Wuqiang Guan[1], Tao Yang[1], Alessandro Furlan[1], Xiong Xiao[1], Kai Yu[1], Xu An[1,7], William Galbavy[1,2], Charu Ramakrishnan[3,4], Karl Deisseroth[3,4], Kimberly Ritola[5], Adam Hantman[5], Miao He[6], Z. Josh Huang[1,7] and Bo Li[1]✉

The basolateral amygdala (BLA) plays essential roles in behaviors motivated by stimuli with either positive or negative valence, but how it processes motivationally opposing information and participates in establishing valence-specific behaviors remains unclear. Here, by targeting *Fezf2*-expressing neurons in the BLA, we identify and characterize two functionally distinct classes in behaving mice, the negative-valence neurons and positive-valence neurons, which innately represent aversive and rewarding stimuli, respectively, and through learning acquire predictive responses that are essential for punishment avoidance or reward seeking. Notably, these two classes of neurons receive inputs from separate sets of sensory and limbic areas, and convey punishment and reward information through projections to the nucleus accumbens and olfactory tubercle, respectively, to drive negative and positive reinforcement. Thus, valence-specific BLA neurons are wired with distinctive input–output structures, forming a circuit framework that supports the roles of the BLA in encoding, learning and executing valence-specific motivated behaviors.

A prevailing model posits that the BLA contains valence-specific neurons that are intrinsically responsive to stimuli of either positive or negative valence (unconditional stimuli (US)), and can drive valence-specific behaviors once activated[1–3]. During learning, initially neutral environmental cues (conditional stimuli (CS)) acquire the capacity to selectively activate these neurons and hence the ability to induce valence-specific behavioral responses[2]. Indeed, previous studies have shown that BLA neurons activated by either appetitive or aversive stimuli, which were targeted on the basis of expression of the immediate early gene *Fos*, are critical for valence-specific behaviors[1,4]. In addition, activation of a population of BLA pyramidal neurons labeled by *Rspo2* (encoding R-spondin 2) or *Cck* (encoding cholecystokinin), two genes that are coexpressed in this population, drives aversive behaviors[5,6], whereas activation of another BLA pyramidal population expressing *Ppp1r1b* (encoding protein phosphatase 1 regulatory inhibitor subunit 1B) drives appetitive behaviors[5]. These findings are consistent with the model and strongly suggest the existence of valence-specific neurons in the BLA.

A recent study measured the in vivo activities of presumptive valence-specific BLA neurons in behaving animals[7]. However, the moment-to-moment relationships between animal behavior and the activity of valence-specific BLA neurons, identified on the basis of either *Fos* or other genetic markers, remain uncharacterized. Such characterization, especially in naturalistic settings where multiple sensory stimuli are available and different behavioral responses can be observed[8], is essential for further understanding the encoding properties of BLA neurons and how these neurons participate in learning or expressing valence-specific behavioral responses. A major obstacle to elucidating the encoding properties and in vivo functions of valence-specific neurons has been a lack of methods to reliably identify these neurons. The *Fos*-based targeting strategy may recruit neurons not relevant to valence, as BLA neurons are sensitive to multiple task features, including sensory properties of individual stimuli and measures of behavioral actions[9]. In addition, this strategy necessitates engaging animals with an aversive or rewarding experience, which may by itself change neuronal properties or responsiveness. Alternatively, previous studies have manipulated BLA neurons on the basis of their projection targets, and shown that activation of BLA neurons projecting to the nucleus accumbens (BLA → NAc), for example, drives appetitive behaviors[3,10–12]. However, recent studies demonstrate that activating a subset of BLA → NAc neurons, which express *Rspo2* or *Cck*, drives aversive behaviors[5,6], suggesting that BLA → NAc neurons contain functionally opposing populations. Indeed, in vivo recording reveals that BLA → NAc neurons, or BLA neurons projecting to other targets, are heterogeneous, containing neurons responsive to stimuli of either positive or negative valence[13,14]. Therefore, projection targets per se may not be sufficient to define valence-specific neurons in the BLA.

The forebrain expressed zinc finger 2 (*Fezf2*) gene encodes a highly conserved master transcription factor that plays an important role in fate specification of layer 5b corticofugal neurons[15–17]. Notably, *Fezf2* is selectively expressed in the BLA within the amygdala complex and is essential for the development of BLA pyramidal neurons[18]. As the BLA and the cortex are evolutionarily and developmentally related[19], it is possible that *Fezf2* also specifies a unique class of pyramidal neurons in the BLA.

[1]Cold Spring Harbor Laboratory, Cold Spring Harbor, NY, USA. [2]Program in Neuroscience, Department of Neurobiology and Behavior, Stony Brook University, Stony Brook, NY, USA. [3]Howard Hughes Medical Institute (HHMI), Stanford University, Stanford, CA, USA. [4]Department of Bioengineering and Department of Psychiatry and Behavioral Sciences, Stanford University, Stanford, CA, USA. [5]Howard Hughes Medical Institute Janelia Research Campus, Ashburn, VA, USA. [6]Institutes of Brain Science, State Key Laboratory of Medical Neurobiology and MOE Frontiers Center for Brain Science, Fudan University, Shanghai, China. [7]Present address: Department of Neurobiology, Duke University School of Medicine, Durham, NC, USA.
✉e-mail: xzhang@cshl.edu; bli@cshl.edu

In this study, we took advantage of the observation that *Fezf2* selectively labels the previously reported *Rspo2*-expressing pyramidal neurons in the anterior basolateral nucleus (BLa) of the BLA complex, and examined how these neurons might encode valences in real time during behavior. Surprisingly, we found that these neurons do not homogeneously represent aversive stimuli as expected from previous studies[5,6]. Rather, these neurons contain two functionally distinct classes, which separately convey punishment or reward information through projections to different ventral striatal nuclei. Thus, genetic identity and projection specificity together allowed us to identify valence-specific BLA neurons, and to uncover how these neurons contribute to the establishment of valence-specific behaviors.

Results

***Fezf2* labels a unique population in the BLA.** To explore the role of *Fezf2*-expressing (*Fezf2*$^+$) neurons in the BLA, we used our newly developed *Fezf2-CreER* and *Fezf2-Flp* knock-in mouse driver lines[20], in which the inducible *Cre* (*CreER*) or the *flippase* (*Flp*) recombinase, respectively, is expressed under the control of endogenous *Fezf2* promoter (Methods). We have previously shown that *Cre*-recombination patterns faithfully recapitulate endogenous *Fezf2* expression patterns in *Fezf2-CreER* mice[20]. Consistent with this finding, single-molecule fluorescence in situ hybridization (smFISH) showed that the expression of *Flp* also recapitulated that of *Fezf2* in the BLA of *Fezf2-Flp* mice (Extended Data Fig. 1a,b). To characterize *Fezf2*$^+$ cells in the BLA, we bred mice harboring the *Fezf2-CreER* allele and an *Ai14* (ref. [21]) or *H2B-GFP*[22] reporter allele expressing the fluorescence protein tdTomato or H2B-GFP (nuclear green fluorescent protein (GFP)), respectively, in a Cre-dependent manner. After tamoxifen induction in these mice (Methods), we found dense fluorescently labeled cells in the BLa, but only sparsely labeled cells in the posterior basolateral nucleus (BLp) of the BLA complex (BLa, 93.5% ± 0.65%; BLp, 6.5% ± 0.65% (four mice); note that BLa and BLp can exist in the same anteroposterior sections; Fig. 1a and Extended Data Figs. 1c and 2). The vast majority (92% ± 2%) of *Fezf2*$^+$ cells in the BLa expressed CaMKII, a marker for excitatory pyramidal neurons[23], but nearly none of them expressed GABA, a marker for inhibitory neurons (Extended Data Fig. 1d–f). In reverse, about 60% of CaMKII$^+$ neurons in the BLa expressed *Fezf2* (Extended Data Fig. 1g), indicating that *Fezf2*$^+$ cells constitute a subset of pyramidal neurons in the BLa.

Recent studies show that activating *Rspo2*$^+$ or *Cck*$^+$ pyramidal neurons in the BLa, which largely belong to the same population, drives aversive behaviors[5,6], whereas activating neurons expressing *Ppp1r1b*, which reside in the BLp, drives appetitive behaviors[5]. We therefore examined the relationship between these populations and *Fezf2*$^+$ neurons in the BLa and BLp using immunohistochemistry and smFISH. Notably, we found that in the BLa virtually all *Fezf2*$^+$ neurons were *Rspo2*$^+$, and none of them were *Ppp1r1b*$^+$ (Fig. 1a,b,d and Extended Data Figs. 2 and 3). In the BLp, *Fezf2*$^+$ neurons were very sparse and were still mainly *Rspo2*$^+$, with only a small fraction being *Ppp1r1b*$^+$ (21%; Fig. 1c,d and Extended Data Figs. 2 and 3). In particular, immunohistochemistry revealed that, in the BLp, only 8% of *Fezf2*$^+$ neurons expressed PPP1R1B, and only 1% of PPP1R1B$^+$ neurons were *Fezf2*$^+$ (Extended Data Fig. 2c). Considering that only 6.5% of *Fezf2*$^+$ neurons are in the BLp (Extended Data Fig. 2b) and the rest are in the BLa where PPP1R1B is essentially absent, the contribution of PPP1R1B$^+$ neurons to the *Fezf2*$^+$ population in BLa and BLp combined is minimal.

Surprisingly, we found that the majority (~70%) of *Rspo2*$^+$ neurons in the BLp were *Ppp1r1b*$^+$ (Fig. 1c,d and Extended Data Fig. 3), contradicting the previous report that *Rspo2*$^+$ neurons and *Ppp1r1b*$^+$ neurons are distinct and spatially segregated in the BLA[5]. Our results thus indicate that, in the BLa, *Fezf2* and *Rspo2* label the same population of pyramidal neurons, which constitute a major population that are distinct from *Ppp1r1b*$^+$ neurons. By contrast, in the BLp, *Fezf2* and *Rspo2* label only sparse populations that are partially overlapping, with the vast majority of *Fezf2*$^+$ neurons having no PPP1R1B or *Ppp1r1b* expression, whereas a substantial fraction of *Rspo2*$^+$ neurons expressed *Ppp1r1b*. Thus, *Fezf2* is superior to *Rspo2* in avoiding labeling (and hence the contamination by) PPP1R1B$^+$ neurons in the BLA.

Fezf2^{BLa} neurons respond to appetitive or aversive stimuli. As recent studies show that optogenetic activation of *Rspo2*$^+$ neurons in the BLa drives innate aversive reactions[5,6], we hypothesized that these neurons homogeneously represent negative valence. To test this hypothesis, we set out to monitor the responses of these neurons to aversive and appetitive stimuli in vivo in behaving animals. To this end, we targeted *Fezf2*$^+$ neurons in the BLa (hereafter referred to as Fezf2^{BLa} neurons) in *Fezf2-CreER* mice, because these neurons are essentially the same as *Rspo2*$^+$ neurons in this location (see above).

We expressed the genetically encoded calcium indicator GCaMP6 (ref. [24]) in Fezf2^{BLa} neurons by injecting the BLa of *Fezf2-CreER* mice with an adeno-associated virus (AAV) expressing GCaMP6f in a Cre-dependent manner, followed by implanting a gradient-index (GRIN) lens into the same location. Four to six weeks after the surgery, the GCaMP6 signals in infected Fezf2^{BLa} neurons were imaged through the GRIN lens with a wide-field microscope (Fig. 2a and Supplementary Fig. 1a,b,d–f). These mice were kept thirsty and were presented with different stimuli, including water and air-puff blowing to the face, as the appetitive and aversive US, respectively, as well as tones of different frequencies, under naïve, awake and head-restraint conditions (Fig. 2b,c and Supplementary Fig. 1a). Hierarchical clustering based on Fezf2^{BLa} neuron response profiles to these stimuli (Methods) revealed two major and distinct populations, with one excited by water but not the air puff, and the other excited by the air puff but not water (Fig. 2b,c and Supplementary Video 1). We termed the former positive-valence neurons (PVNs) and the latter negative-valence neurons (NVNs). Only a few Fezf2^{BLa} neurons responded to the tones (Fig. 2h). Interestingly, PVNs and NVNs, as well as all other

Fig. 1 | *Fezf2* selectively labels a unique pyramidal neuron population in the BLA. a, Confocal images of coronal brain sections containing the BLa from a representative *Fezf2-CreER;Ai14* mouse, showing the distribution of *Fezf2*$^+$ neurons labeled with tdTomato, and the distribution of Ppp1r1b expression detected with antibodies. High-magnification images of the boxed area in the corresponding overlay image are shown on the right. These images are the same as those at AP −1.34 mm in Extended Data Fig. 2. This experiment was repeated in four mice. **b**, Upper, confocal images of coronal brain sections containing the BLa from a representative *Fezf2-CreER;H2B-GFP* mouse, showing the distribution of *Fezf2*$^+$ neurons labeled with H2B-GFP, and the distribution of *Rspo2* and *Ppp1r1b* expression detected with smFISH. Lower, high-magnification images of the boxed area in the upper overlay image. These images are the same as those at AP −1.34 mm in Extended Data Fig. 3a. This experiment was repeated in two mice. **c**, Same as **b**, except that the images include BLp. These images are the same as those at AP −2.06 mm in Extended Data Fig. 3a. **d**, Quantification of the overlap between neurons that express *Fezf2*, *Rspo2* and *Ppp1r1b* detected with smFISH in the BLa (left) and BLp (right). Each value in parentheses represents the number of neurons detected with the respective probe in two mice. Values in the matrix represent the percentage labeling with probes in columns among neurons labeled with probes in rows. For example, in the BLa (left), 98% of *Fezf2*-labeled neurons were also labeled with *Rspo2*. BMA, basomedial amygdala; CeL, central amygdala lateral part; ITC, intercalated cells of the amygdala; LA, lateral amygdalar nucleus.

Fezf2^{BLa} neurons including a small population that was excited by both water and the air puff (Fig. 2d), were intermingled with no obvious spatial clustering (Fig. 2e).

Importantly, we targeted the viral injections to the BLa, which is devoid of PPP1R1B expression. In addition, as described above, the contribution of PPP1R1B^{+} neurons to the *Fezf2*$^{+}$ population

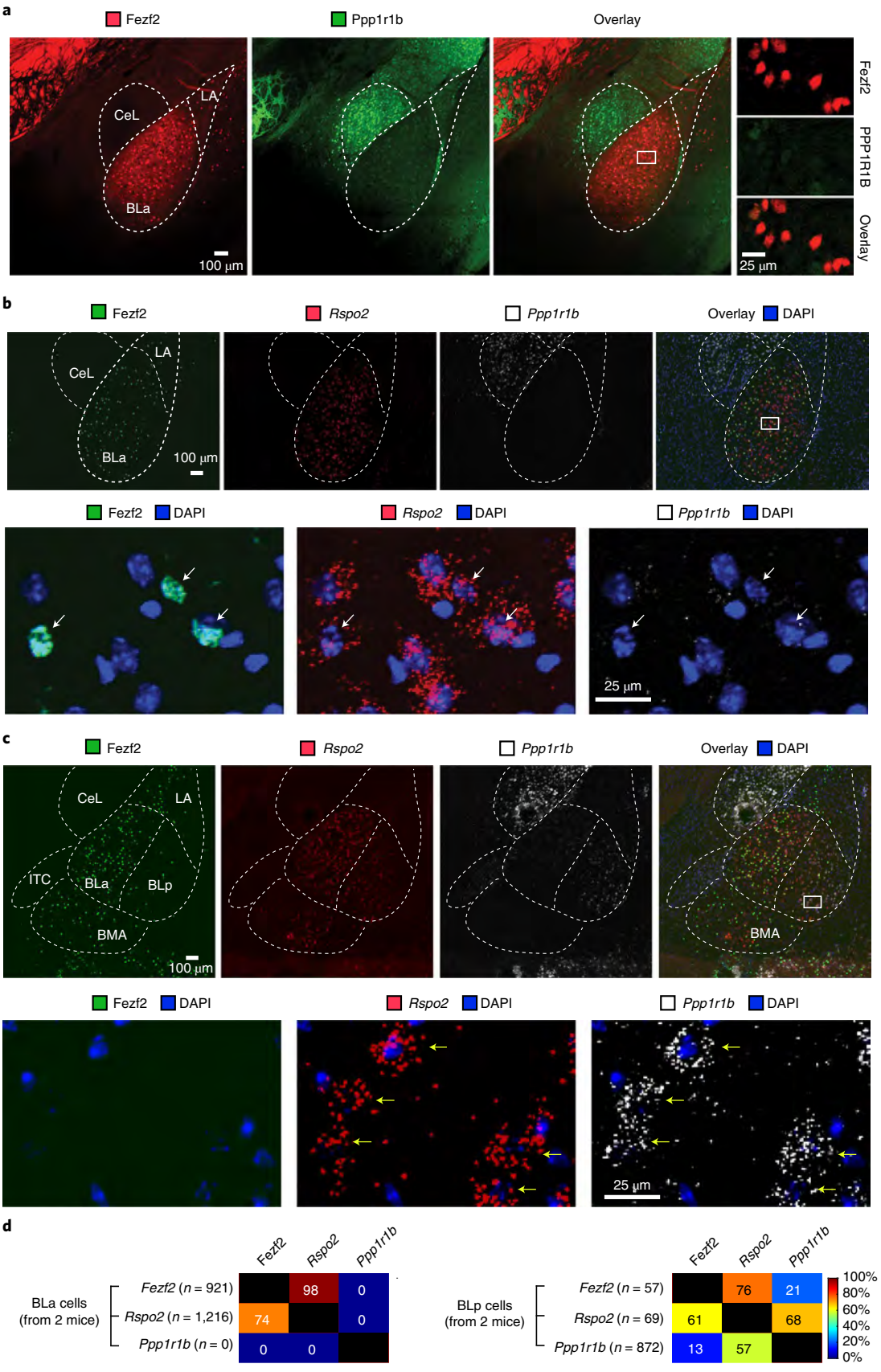

was minimal even if both the BLa and BLp were considered. Thus, the PVNs we imaged unlikely represent PPP1R1B$^+$ neurons, which have been reported to process appetitive stimuli[5,25]. We conclude that Fezf2^{BLa} (or Rspo2^{BLa}) neurons are functionally heterogeneous; they encode either positive or negative valence, rather than homogeneously represent negative valence.

***Fezf2*$^-$ BLa neurons are sensitive to auditory stimuli.** As a comparison, we also imaged the activities of *Fezf2*-negative (*Fezf2*$^-$) BLa pyramidal neurons, which were labeled by injecting the BLa of *Fezf2-Flp* mice with an AAV expressing GCaMP6 only if Flp is not present (Flp-off[26]; Supplementary Fig. 1a,c,d,h,i). Interestingly, in contrast to *Fezf2*$^+$ BLa neurons, a major fraction of *Fezf2*$^-$ BLa neurons showed prominent responses specifically to the auditory stimuli, whereas only small fractions of these neurons showed valence-specific responses or mixed encoding (Fig. 2f–h). Our results suggest that *Fezf2*$^+$ and *Fezf2*$^-$ BLa neurons have distinct functional roles, with the former sensitive to valence and the latter tuned in to auditory stimuli.

CS responses evolve in Fezf2^{BLa} neurons during learning. To test how Fezf2^{BLa} neurons might participate in the development of behaviors motivated by positive and negative valences, we designed an 'active approach and avoidance' (AAA) task, in which mice learned to both actively seek reward and actively avoid punishment (Fig. 3a and Methods). There were three types of trials in this task–reward, punishment and neutral–which were randomly interleaved. In the reward trials, a sound (CS_R) indicated that water would be delivered, but only if mice licked the water spout during a decision window following the CS. In the punishment trials, another sound (CS_P) announced that an air puff would be delivered, but mice could avoid the air puff by running during the decision window. In the neutral trials, a third sound (CS_N) indicated that nothing would happen (Fig. 3a). Early during training, mice rarely licked or ran during the decision window, and thus failed to obtain water or avoid the air puff in most of the cases; late in training, however, mice were able to acquire appropriate actions, licking during the decision window only in reward trials to obtain water, and running during the decision window specifically in punishment trials to avoid the air puff (Fig. 3b, Extended Data Fig. 4a–d and Supplementary Fig. 2).

Early during training in the AAA task, only a small fraction of Fezf2^{BLa} neurons responded to any of the CS (Fig. 3c–e and Extended Data Fig. 4e), consistent with the observation that not many Fezf2^{BLa} neurons responded to tones in naïve mice (Fig. 2h). At this stage, reward responses in these neurons were also rare, but this was because animals failed to obtain water in most of the reward trials (Extended Data Fig. 4a,b). Late in training, when the mice have achieved high performance in this task, the number of Fezf2^{BLa} neurons excited by either CS_R or CS_P was substantially increased, whereas the number excited by CR_N remained unchanged (Fig. 3c–e and Extended Data Fig. 4f). At this stage, punishment responses in these neurons were rare, because animals successfully avoided the air puff in most of the punishment trials (Extended Data Fig. 4c,d). Very few Fezf2^{BLa} neurons were inhibited by the CS throughout training (Fig. 3d). Notably, the neurons excited by CS_R or CS_P after learning were largely nonoverlapping (Fig. 3e) and could be classified into two distinct groups corresponding to NVNs and PVNs by unsupervised hierarchical clustering (Extended Data Fig. 4g,h). These results indicate that learning increases the size of two functionally distinct Fezf2^{BLa} populations, with one excited by the CS predicting reward, whereas the other excited by the CS predicting punishment.

To determine how the CS responses in Fezf2^{BLa} neurons evolve during learning, we first examined if the neurons excited by CS after learning were also excited by the entraining US. We identified the neurons selectively excited by either CS_R or CS_P at the late training stage in the AAA task, and assessed how they responded to either signaled or un-signaled delivery of reward (US_R) and punishment (US_P). We found that the majority of the CS-excited neurons were specifically excited by the entraining US but not the other US, and thus belonged to either PVNs or NVNs (74% of the CS_R-excited neurons were excited by US_R but not US_P; 72% of the CS_P-excited neurons were excited by US_P but not US_R; Fig. 3f,g). There was also a fraction of US_R-excited or US_P-excited neurons that remained nonresponsive to CS_R or CS_P (the US_R-only or US_P-only neurons; Fig. 3g).

Next, we tracked the activities of the same neurons in multiple sessions spanning the early and late training stages (session (S)1, S12, S29 and S42; one session per day; Fig. 3h,i and Methods). There was a total of 45 Fezf2^{BLa} neurons traceable in all the four sessions. Among these neurons, four developed excitatory responses selectively to CS_R and six developed excitatory responses selectively to CS_P during training, with the responses being detectable from S12 and increasing in the subsequent sessions. Notably, all the tracked CS_R-excited neurons showed an excitatory response to US_R but not US_P; in a similar fashion, all the tracked CS_P-excited neurons showed an excitatory response to US_P but not US_R (Fig. 3h,i). Moreover, the valence-specific US response in these neurons was maintained from before training to late in training. Together, these results suggest that, during learning, valence-specific CS response emerges in a subpopulation of Fezf2^{BLa} neurons showing intrinsic, valence-specific response to the entraining US.

Fezf2^{BLa} CS response correlates and predicts behavior. To determine if the CS responses of Fezf2^{BLa} neurons can be used to guide behavior, we assessed their relationship to valence-specific actions. We found that, first, the appearance and development of CS_R or CS_P

Fig. 2 | Characterization of *Fezf2*$^+$ and *Fezf2*$^-$ neuron response properties. a, Left, the field of view of GCaMP6f signals from *Fezf2*$^+$ BLa neurons through a GRIN lens. Right, the spatial locations of individual extracted neurons (N, NVN; P, PVN; O, other neurons). The contours of neurons showing the excitatory response to water, air puff or both stimuli, and the contours of the 'other' neurons showing either inhibitory response to the two stimuli or only spontaneous responses, were outlined and color coded. The numbers indicate the corresponding example neurons in Supplementary Video 1. The letters indicate the corresponding representative neurons in **b**. **b**, Trial-by-trial responses of three representative *Fezf2*$^+$ neurons to different stimuli. **c**, Heat maps of the activities (*z*-scores) in individual *Fezf2*$^+$ neurons from all mice ($n = 10$), in trials where the following stimuli were presented (from left to right): 4,000-Hz tone, 12,000-Hz tone, water and air puff. Stimulus onset Is indicated by the dashed line. Each row represents the temporal activities of the same neuron. Neurons were sorted by hierarchical clustering based on their response profiles. **d**, Pie graph showing the percentage distribution of *Fezf2*$^+$ neurons excited by different US. **e**, Cumulative probability distributions of centroid distances between pairs of cells from the entire population ('all'), between pairs of cells that were excited by the water reward ('water'), and between pairs of cells that were excited by the aversive air puff ('air puff') in each of the 10 mice (all versus water, $P = 0.16$; all versus air puff, $P = 0.19$; Kolmogorov–Smirnov test). Inset, the corresponding probability densities. **f**, Trial-by-trial responses of five representative *Fezf2*$^-$ neurons to different stimuli. NR, nonresponsive. **g**, Same as **c**, except that activities of *Fezf2*$^-$ neurons ($n = 5$ mice) were used for analysis. **h**, Quantification of the proportions of *Fezf2*$^+$ neurons ($n = 10$ mice) or *Fezf2*$^-$ neurons ($n = 5$ mice) showing excitatory responses to different stimuli ($F(3, 39) = 44.16$, $P < 0.0001$, $^{****}P < 0.0001$, two-way repeated measures analysis of variance (ANOVA) followed by Bonferroni's multiple-comparisons test). Data are presented as the mean ± s.e.m.

responses were accompanied by the emergence and development of reward-seeking (licking) or punishment-avoidance (running) behavior, respectively, in the AAA task (Fig. 3i). Second, by separately analyzing the CS responses in success trials and failure trials in the AAA task, we found that PVNs had larger CS_R responses in trials where mice successfully obtained reward than trials in which mice failed to obtain the reward (Fig. 4a). In parallel, NVNs had larger CS_P responses in trials where mice successfully avoided punishment than trials in which mice failed to avoid the punishment (Fig. 4b). Third, change-point analysis[27,28] revealed that the CS_R responses in most PVNs preceded reward seeking, while the CS_P responses in most NVNs preceded punishment avoidance (Fig. 4c,d). These results suggest that the CS responses of these neurons can be used to guide the animals' behavior.

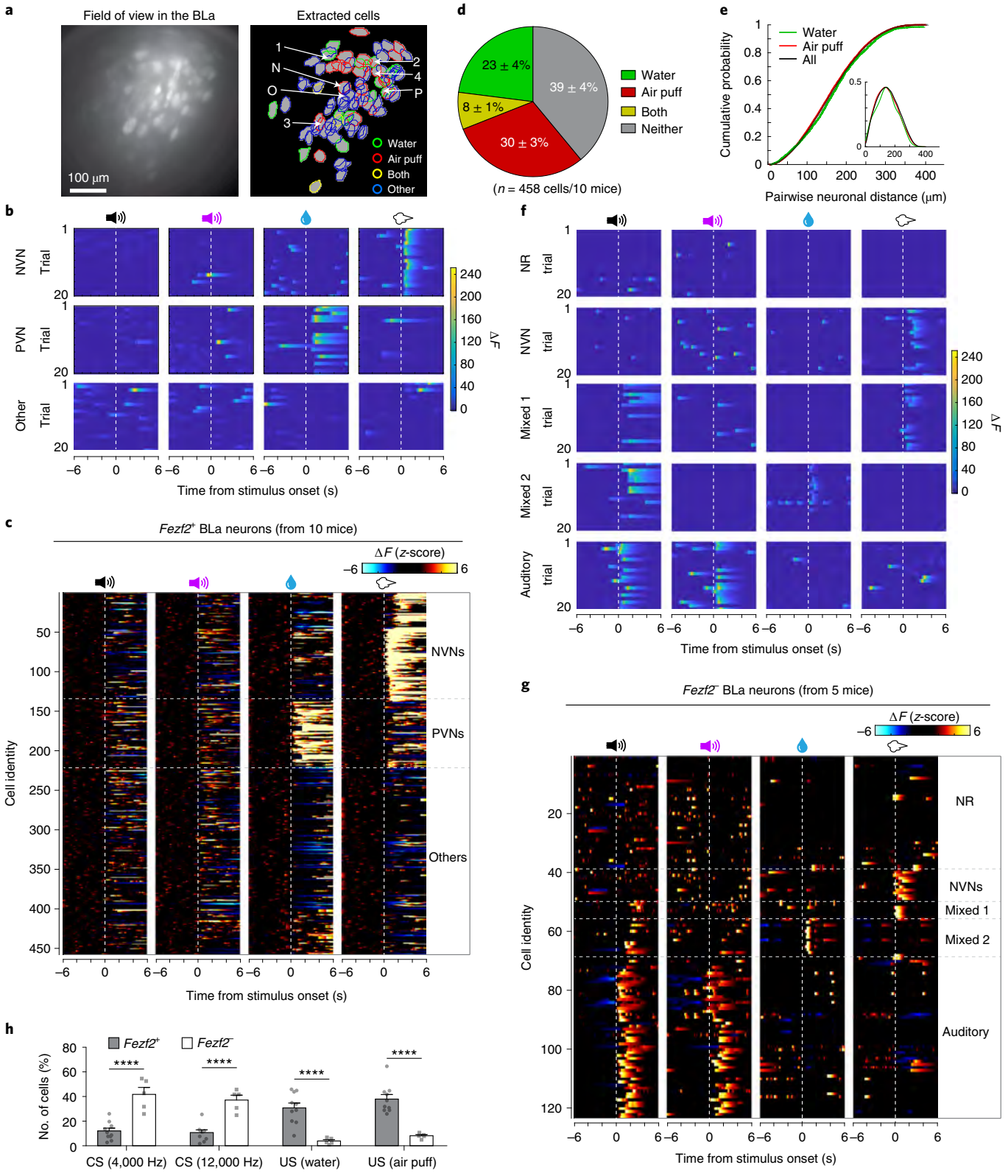

To further test this idea, we performed trial-by-trial analysis on Fezf2^{BLa} neuronal population activities after dimensionality reduction[29] (Methods). We found that, after learning, the trajectories of the dynamic population activities during CS presentation in trials of different types (reward, punishment and neutral) were clearly separable (Fig. 4e), suggesting that these activities predict the trial type. Indeed, the population CS responses of Fezf2^{BLa} neurons after learning could be used to accurately decode the three trial types (Fig. 4f,g). Such features of Fezf2^{BLa} neurons were not present before learning (Fig. 4e,g). Together, these findings point to the possibility that the learning-induced CS responses in Fezf2^{BLa} neurons can inform the type or the valence of an incoming US, and thus guide or promote reward seeking and punishment avoidance.

Fezf2^{BLa} neurons project to distinct ventral striatal areas. We reasoned that the function of Fezf2^{BLa} neurons in reward seeking or punishment avoidance is mediated by their projections to downstream targets. To identify the targets, we first used an anterograde tracing strategy in which we expressed GFP selectively in Fezf2^{BLa} neurons of *Fezf2-CreER* mice, and searched for areas containing GFP-labeled axons in the whole brain (Fig. 5a–c and Extended Data Fig. 5a–c). We found four major areas that contained visible labeled axons, the NAc, olfactory tubercle (OT), medial prefrontal cortex (mPFC) and lateral septum (LS), with the NAc and OT having the densest labeling (Fig. 5c and Extended Data Fig. 5a–c).

As the NAc and OT are two ventral striatum structures that have been extensively implicated in reward-driven or punishment-driven behaviors[30,31], we further characterized the projections to these two structures. To selectively label Fezf2^{BLa} neurons projecting to the NAc (Fezf2$^{BLa\rightarrow NAc}$) or OT (Fezf2$^{BLa\rightarrow OT}$), we used an intersectional strategy, in which we injected the NAc or OT of *Fezf2-Flp* mice with a retrograde AAV (AAVrg) expressing Cre in a Flp-dependent manner (fDIO), and injected the BLa of the same mice with an AAV expressing GFP in a Cre-dependent manner (Extended Data Fig. 5d,g). We found that Fezf2$^{BLa\rightarrow NAc}$ neurons sent stronger projections to the NAc than OT, mPFC and LS (Extended Data Fig. 5e,f), while Fezf2$^{BLa\rightarrow OT}$ neurons sent stronger projections to the OT than NAc, mPFC and LS (Extended Data Fig. 5h,i). These results suggest that Fezf2$^{BLa\rightarrow NAc}$ and Fezf2$^{BLa\rightarrow OT}$ neurons preferentially project to the NAc and OT, respectively.

To assess the degree of overlap between Fezf2$^{BLa\rightarrow NAc}$ and Fezf2$^{BLa\rightarrow OT}$ populations, we used *Fezf2-CreER;H2B-GFP* mice, in which Fezf2^{BLa} neurons were labeled with the nuclear GFP, H2B-GFP, and injected the NAc and OT in the same animals with the retrograde tracer cholera toxin subunit B (CTB) conjugated with different fluorophores (Extended Data Fig. 5j). This approach, which allows identification of Fezf2$^{BLa\rightarrow NAc}$ and Fezf2$^{BLa\rightarrow OT}$ neurons in the same animals, revealed that there was little overlap between these two populations (Extended Data Fig. 5k,l). To verify this result with a different type of tracer, we injected the NAc or OT of the *Fezf2-CreER* mice with an AAVrg expressing GFP or mCherry, respectively, in a Cre-dependent manner (Extended Data Fig. 6a,b). This approach, which again allowed identification of Fezf2$^{BLa\rightarrow NAc}$ and Fezf2$^{BLa\rightarrow OT}$ neurons in the same animals, confirmed that there were only small portions of overlapping neurons in these two populations (Extended Data Fig. 6c).

The retrograde tracing with AAVrg, combined with immunohistochemistry, also revealed that the vast majority of either Fezf2$^{BLa\rightarrow NAc}$ (93% ± 2.5%) or Fezf2$^{BLa\rightarrow OT}$ (92% ± 2.4%) neurons were localized to the BLa, and none of these neurons expressed PPP1R1B; moreover, even among the 7–8% of either Fezf2$^{BLa\rightarrow NAc}$ or Fezf2$^{BLa\rightarrow OT}$ neurons localized to the BLp, only 10% expressed PPP1R1B (Extended Data Fig. 6d,e). These results thus confirm that the vast majority of BLA *Fezf2*$^{+}$ neurons are located in the BLa and do not express PPP1R1B, irrespective of their projection targets.

Next, we examined the functional connectivity between Fezf2^{BLa} neurons and neurons in the NAc or OT (Extended Data Fig. 7). Using the intersectional strategy described above (Extended Data Fig. 5d,g), we expressed the light-gated cation channel channelrhodopsin (ChR2) selectively in Fezf2$^{BLa\rightarrow NAc}$ or Fezf2$^{BLa\rightarrow OT}$ neurons (Extended Data Fig. 7a,f). We prepared acute brain slices from these mice, in which we recorded monosynaptic responses (in the presence of TTX and 4-AP[32]) in randomly chosen NAc or OT neurons to photoactivation of the axons originating from Fezf2$^{BLa\rightarrow NAc}$ or Fezf2$^{BLa\rightarrow OT}$ neurons (Extended Data Fig. 7b,g). The majority of NAc or OT neurons showed detectable light-evoked synaptic responses, suggesting high levels of functional connectivity (Extended Data Fig. 7c,d,h,i). Notably, photoactivation of Fezf2$^{BLa\rightarrow NAc}$ axons drove much larger synaptic responses in NAc neurons than OT neurons (Extended Data Fig. 7c,e). By contrast, photoactivation of Fezf2$^{BLa\rightarrow OT}$ axons drove responses of equivalent amplitude in NAc or OT neurons (Extended Data Fig. 7h,j).

Together, the anterograde and retrograde tracing results indicate that Fezf2$^{BLa\rightarrow NAc}$ and Fezf2$^{BLa\rightarrow OT}$ neurons represent two largely nonoverlapping populations that preferentially project to the NAc and OT, respectively. The functional circuit-mapping results provide further support that Fezf2$^{BLa\rightarrow NAc}$ neurons preferentially innervate NAc neurons (Extended Data Fig. 5d–f), but also reveal that Fezf2$^{BLa\rightarrow OT}$ neurons drive synaptic responses of similar amplitude in OT and NAc neurons. The latter finding suggests that even sparse projections in the NAc can have a functional impact, considering that only a small portion of Fezf2$^{BLa\rightarrow OT}$ neurons send collaterals to the NAc (Extended Data Figs. 5j–l and 6a–c) and the collaterals are relatively sparse (Extended Data Fig. 5g–i).

Fezf2$^{BLa\rightarrow NAc}$ and Fezf2$^{BLa\rightarrow OT}$ represent opposing valences. The capacity of retrograde tracing in labeling largely nonoverlapping Fezf2$^{BLa\rightarrow NAc}$ and Fezf2$^{BLa\rightarrow OT}$ neurons (Extended Data Figs. 5j–l and 6a–c) allowed us to investigate whether these two populations are differentially involved in reward seeking and punishment avoidance. We first monitored the responses of each of these populations

Fig. 3 | Learning induces valence-specific predictive responses in Fezf2^{BLa} neurons. a, A schematic of the task. **b**, Quantification of licking (left) and running (right) during the decision window ($n = 10$; licking, F-stat 28.04, $P < 0.0001$; CS_R, $^*P = 0.014$; CS_N, $P = 0.90$; CS_P, $P = 0.68$; running, F-stat 24, $P < 0.0001$; CS_R, $P = 0.99$; CS_N, $P = 0.99$; CS_P, $^*P = 0.012$; Friedman test with Dunn's post hoc test). **c**, Responses of six representative neurons during early (top) and late (bottom) training stages. **d**, Quantification of the percentage of neurons selectively excited (top) or inhibited (bottom) by different CS ($n = 10$; excited, F-stat 34.04, $P < 0.0001$; CS_R, $^*P = 0.018$; CS_N, $P = 0.99$; CS_P, $^{****}P < 0.0001$; inhibited, F-stat 5.02, $P = 0.41$; CS_R, $P = 0.99$; CS_N, $P = 0.99$; CS_P, $P = 0.99$; Friedman test with Dunn's post hoc test). **e**, Venn diagrams show the percentage distributions of neurons at early (upper) and late (lower) training stages. Numbers on the side indicate the percentage of CS-excited, CS-inhibited or nonresponsive neurons. **f**,**g**, Data from the late stage. **f**, Top, activity traces of neurons excited by only CS_R (left), both CS_R and US_R (middle) or only US_R (right). The latter two belong to PVNs. Bottom, activity traces of neurons excited by only CS_P (left), both CS_P and US_P (middle) or only US_P (right). The latter two belong to NVNs. **g**, Pie graphs showing the percentage distributions of different types of neurons. **h**, Raw image projections acquired in different sessions (S1, S12, S29 and S42) from a representative mouse (top), and positioning of extracted cells in the corresponding images after alignment (bottom). Neurons detected in all sessions are indicated in green. **i**, Responses of cell 1 (PVN) and cell 2 (NVN), which correspond to the two cells indicated by arrows in **h**, in reward and punishment trials, respectively, across different training sessions. The corresponding behavioral responses (licking or running) of the mouse are also plotted. Data are presented as the mean ± s.e.m. Shaded areas around traces represent the s.e.m. NS, not significant.

to appetitive and aversive stimuli. For this purpose, we expressed GCaMP6 selectively in Fezf2$^{BLa\rightarrow NAc}$ or Fezf2$^{BLa\rightarrow OT}$ neurons by injecting the NAc or OT, respectively, of *Fezf2-CreER* mice with an AAVrg expressing GCaMP6 in a Cre-dependent manner. This virus had relatively low expression levels of GCaMP6, resulting in dim fluorescence signals that precluded us from resolving single neurons with GRIN lens-based imaging. To address this issue, we used fiber photometry[33,34] to record bulk GCaMP6 signals from the infected Fezf2$^{BLa\rightarrow NAc}$ or Fezf2$^{BLa\rightarrow OT}$ neurons through optical fibers implanted in the BLa in these mice (Fig. 5d and Supplementary Fig. 3). Notably, we found that Fezf2$^{BLa\rightarrow NAc}$ neurons were activated by aversive stimuli, including air puffs and tail shocks, but were

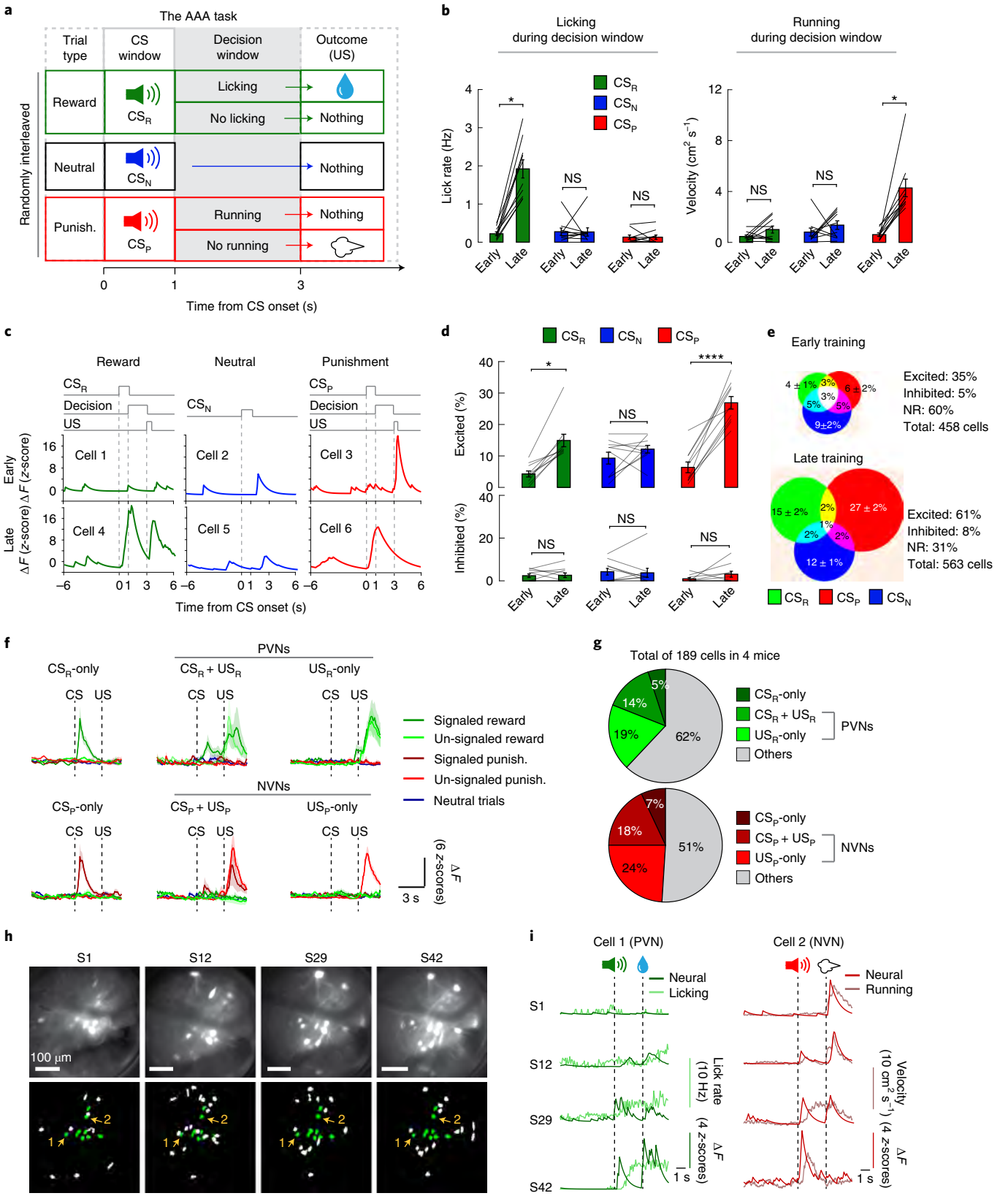

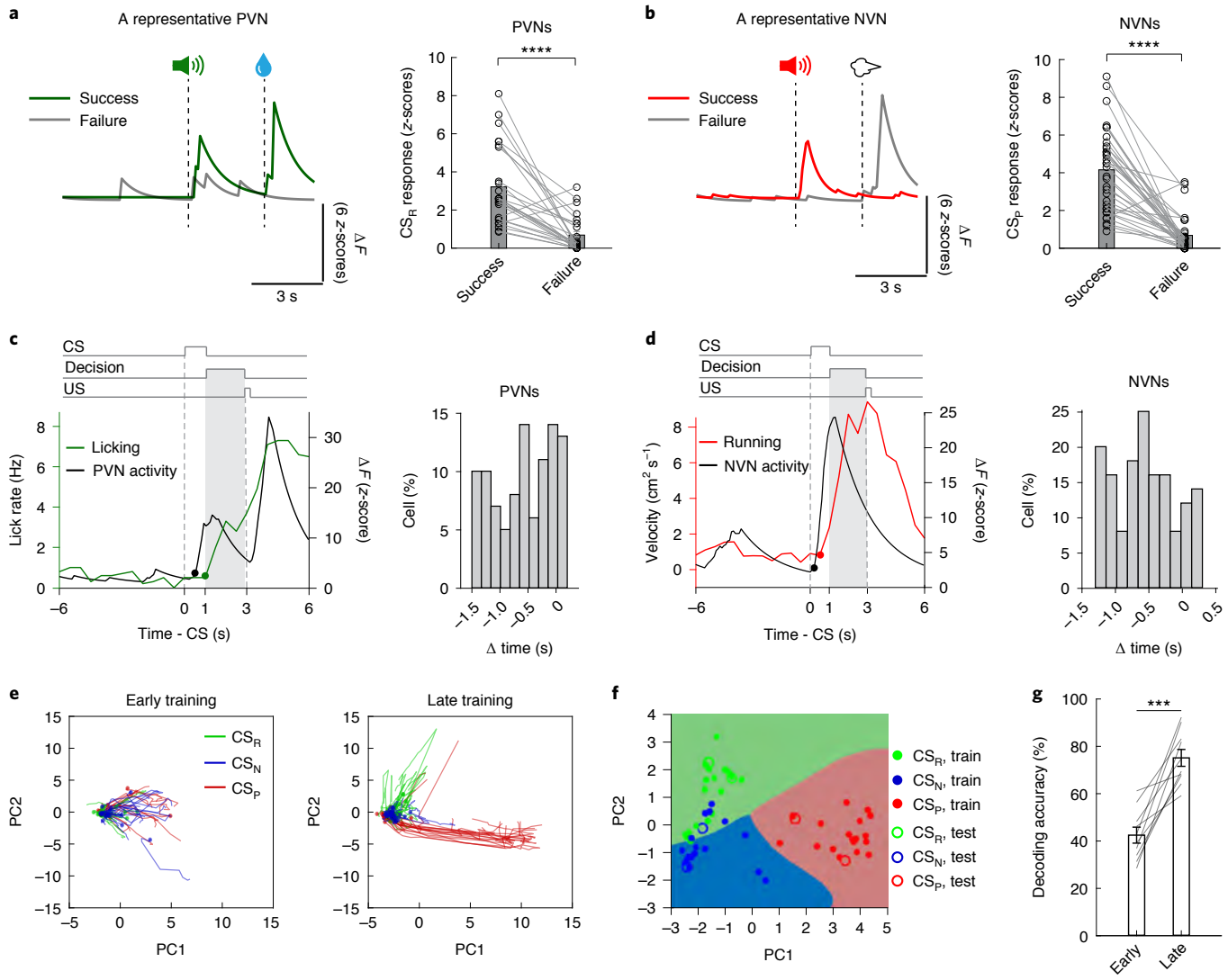

Fig. 4 | Fezf2^{BLa} neuron activity predicts reward seeking and punishment avoidance. a, Left, activity traces of a representative PVN in reward trials, with average activities in success and failure trials plotted separately. Right, quantification of CS_R responses of all PVNs in success and failure trials ($n=26$, $t_{(25)}=5.8$, $^{****}P=9.4\times10^{-6}$; paired *t*-test with Bonferroni correction). **b**, Left, activity traces of a representative NVN in punishment trials, with average activities in success and failure trials plotted separately. Right, quantification of CS_P responses of all NVNs in success and failure trials ($n=34$, $t_{(33)}=8.7$, $^{****}P=1\times10^{-9}$; paired *t*-test with Bonferroni correction). **c**, Left, the timing of increase in activity in a representative PVN, and that of increase in licking response of the corresponding mouse after CS_R onset, as determined by change-point analysis. Right, quantification of the difference between neural and behavioral change points, for all PVNs and the corresponding mice. Values below zero indicate that neural responses precede behavioral responses. **d**, Same as in **c**, except that neural responses in NVNs and running behavior after CS_P onset were analyzed. **e**, Trial-by-trial population CS responses in a representative mouse in early (left) and late (right) training stages in the AAA task. The responses are plotted in a two-dimensional (2D) space after dimensionality reduction with principal-component analysis (PCA). Each line represents one trial. Dots indicate CS onset. **f**, Performance of a support vector machine (SVM) classifier, trained with population CS responses, in predicting trial types (reward, green; punishment, red; neutral, blue). **g**, Learning increased decoding accuracy ($n=10$ mice; $t(9)=-6.4$, $^{***}P=1.3\times10^{-4}$; paired *t*-test). Data are presented as the mean ± s.e.m.

nonresponsive to appetitive stimuli, such as water, fat or sucrose solution (Fig. 5e,f). By contrast, Fezf2$^{BLa\rightarrow OT}$ neurons were excited by the appetitive stimuli but not the aversive stimuli (Fig. 5e,f). These results suggest that Fezf2$^{BLa\rightarrow NAc}$ and Fezf2$^{BLa\rightarrow OT}$ neurons represent negative and positive valence, respectively, and convey the respective valence information to the NAc and OT.

Next, we trained these mice in the AAA task as above (Fig. 3a), and recorded the activities of Fezf2$^{BLa\rightarrow NAc}$ or Fezf2$^{BLa\rightarrow OT}$ neurons at both early and late training stages with fiber photometry. We found that, at the early stage, when the performance of the mice was poor, neither population showed obvious responses to CS_R and CS_P (Fig. 5g–j). By contrast, at the late stage, when mice had achieved high performance, Fezf2$^{BLa\rightarrow NAc}$ neurons were excited by CS_P but not CS_R, whereas Fezf2$^{BLa\rightarrow OT}$ neurons were excited by CS_R but not CS_P. Neither Fezf2$^{BLa\rightarrow NAc}$ nor Fezf2$^{BLa\rightarrow OT}$ neurons showed a response to CS_N (Fig. 5g–j). These results are consistent with the observation from GRIN lens imaging that valence-specific predictive responses evolve in the NVNs and PVNs, and moreover map the responses onto Fezf2$^{BLa\rightarrow NAc}$ and Fezf2$^{BLa\rightarrow OT}$ neurons.

Fezf2$^{BLa\rightarrow NAc}$ and Fezf2$^{BLa\rightarrow OT}$ have distinct synaptic inputs. Because Fezf2$^{BLa\rightarrow NAc}$ and Fezf2$^{BLa\rightarrow OT}$ neurons are strikingly dif-

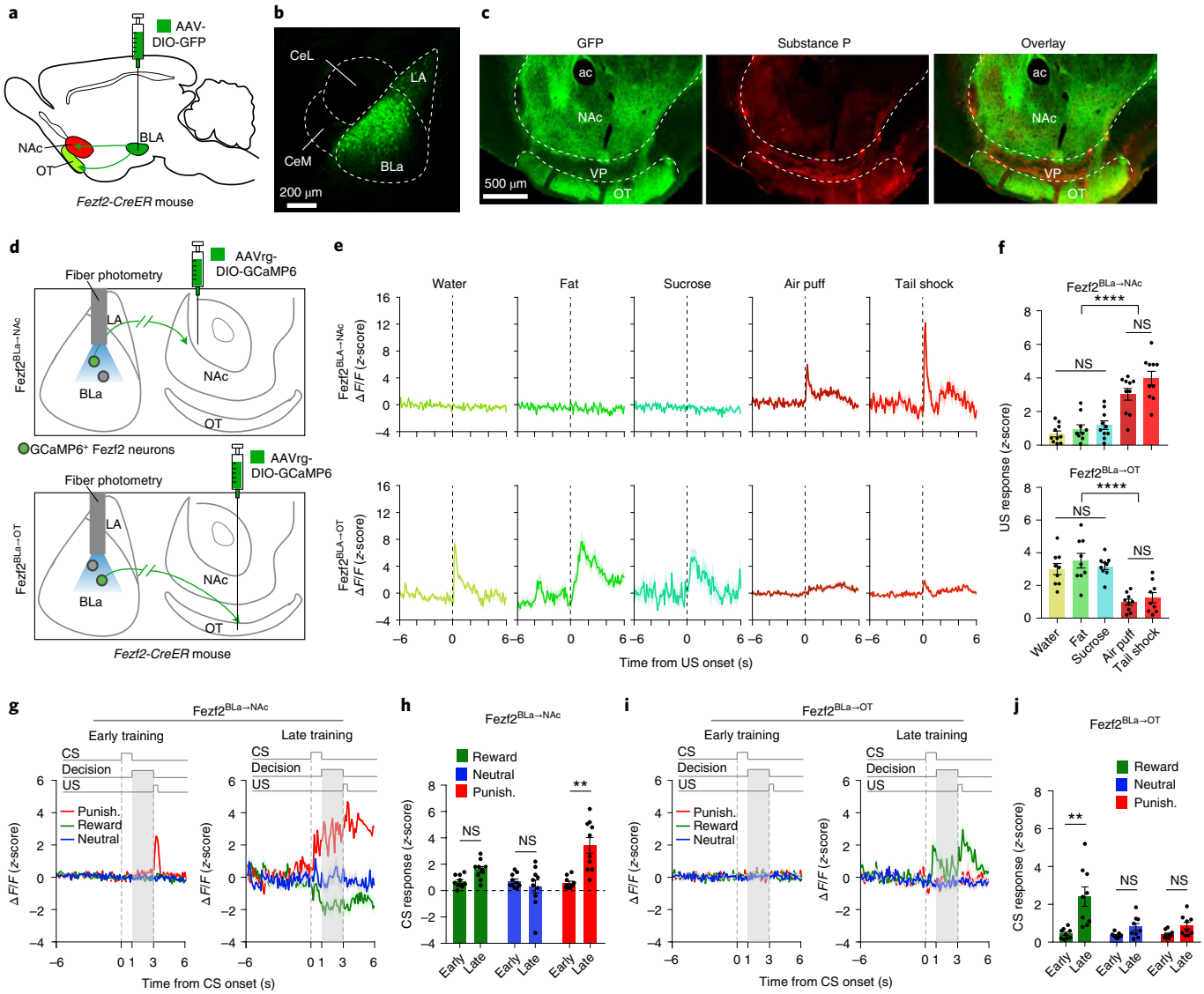

Fig. 5 | Predictive valence-specific signals evolve in Fezf2$^{BLa\rightarrow NAc}$ and Fezf2$^{BLa\rightarrow OT}$ neurons during learning. a, A schematic of the approach. **b**, A representative confocal image showing the infection of Fezf2^{BLa} neurons with an AAV expressing GFP. This experiment was repeated in four mice. **c**, Confocal images showing GFP-labeled axons originating from Fezf2^{BLa} neurons (left), antibodies recognizing substance P used to label the ventral pallidum (VP; middle) and an overlay image (right). This experiment was repeated in four mice. **d**, Schematics of the approach. **e**, Upper, the responses of Fezf2$^{BLa\rightarrow NAc}$ neurons in an example mouse to different stimuli. Lower, the responses of Fezf2$^{BLa\rightarrow OT}$ neurons in an example mouse to different stimuli. **f**, Upper, quantification of the responses of Fezf2$^{BLa\rightarrow NAc}$ neurons in all mice to different stimuli ($n=10$ mice; $F(4, 45)=23.96$, $P<0.0001$; $^{****}P<0.0001$; NS, $P>0.05$; one-way ANOVA followed by Tukey's multiple-comparisons test). Lower, quantification of the responses of Fezf2$^{BLa\rightarrow OT}$ neurons in all mice to different stimuli ($n=9$ mice; $F(4, 40)=14.1$, $P<0.0001$; $^{****}P<0.0001$, NS, $P>0.05$; one-way ANOVA followed by Tukey's multiple-comparisons test). **g**, The responses of Fezf2$^{BLa\rightarrow NAc}$ neurons in an example mouse in the AAA task during early (left) and late (right) training stages. **h**, Quantification of the responses of Fezf2$^{BLa\rightarrow NAc}$ neurons in all mice to different CS during learning in the AAA task ($n=10$ mice; Friedman test (F-stat 22.7) with Dunn's post hoc test, $P=0.0004$; CS_R, $P=0.13$; CS_N, $P=0.99$; CS_P, $^{**}P=0.004$). **i**, The responses of Fezf2$^{BLa\rightarrow OT}$ neurons in an example mouse in the AAA task during early (left) and late (right) training stages. **j**, Quantification of the responses of Fezf2$^{BLa\rightarrow OT}$ neurons in all mice to different CS during learning in the AAA task ($n=9$ mice; Friedman test (F-stat 25.48) with Dunn's post hoc test, $P=0.0001$; CS_R, $^{**}P=0.0018$; CS_N, $P=0.56$; CS_P, $P=0.35$). Data are presented as the mean ± s.e.m. CeM, central amygdala medial part.

ferent in their responses to stimuli of positive or negative valence, it is likely that these two populations are innervated by different synaptic inputs. To test this possibility, we mapped brain-wide monosynaptic inputs onto each of these populations (Fig. 6a–i and Supplementary Figs. 4 and 5). To achieve this goal, we first injected the NAc or OT of *Fezf2-CreER* mice with a retrograde virus CAV-Flex-Flp[35] (Fig. 6a,e), which allowed Flp to be specifically expressed in Fezf2$^{BLa\rightarrow NAc}$ or Fezf2$^{BLa\rightarrow OT}$ neurons, respectively, following tamoxifen induction. We then infected these neurons with a Flp-dependent rabies virus system[34,36–39] (Fig. 6a,e, Supplementary Fig. 4a–h and Methods).

This approach revealed marked differences between the inputs onto Fezf2$^{BLa\rightarrow NAc}$ neurons and those onto Fezf2$^{BLa\rightarrow OT}$ neurons (Fig. 6i and Supplementary Figs. 4i,j and 5). In particular, Fezf2$^{BLa\rightarrow NAc}$ neurons receive inputs from the paraventricular nucleus of the thalamus (PVT), the cortical amygdala (CoA) and dorsal raphe (DR; Fig. 6d,i). These areas send only weak or no output to innervate Fezf2$^{BLa\rightarrow OT}$ neurons (Fig. 6h,i). By contrast,

Fezf2$^{BLa\rightarrow OT}$ neurons receive substantial inputs from the piriform cortex (PIR) and the ventral part of the medial geniculate complex (MGv; Fig. 6h,i), which send no or weak output to innervate Fezf2$^{BLa\rightarrow NAc}$ neurons (Fig. 6d,i). There were several other areas (for example, posterior intralaminar nucleus of the thalamus (PIL) and entorhinal area (ENT)) showing differential innervation of Fezf2$^{BLa\rightarrow NAc}$ versus Fezf2$^{BLa\rightarrow OT}$ neurons, although the differences did not reach significance when corrected for multiple comparisons (Fig. 6i). Thus, Fezf2$^{BLa\rightarrow NAc}$ and Fezf2$^{BLa\rightarrow OT}$ neurons not only preferentially project to different targets, but also receive inputs from distinct sets of sensory and limbic structures that may determine, at least in part, their distinct response properties and functions.

Fezf2^{BLa} activity is required for approach and avoidance. To determine if the activity of Fezf2^{BLa} neurons is causally linked to reward seeking or punishment avoidance, we began by inhibiting these neurons— irrespective of their projection targets—in mice that had learned the AAA task (Extended Data Fig. 8a–k). To achieve selective and reversible inhibition of Fezf2^{BLa} neurons, we expressed in these neurons an inhibitory DREADD (designer receptor exclusively activated by designer drug) by bilaterally injecting the BLa of *Fezf2-CreER* mice with an AAV expressing KORD (a DREADD derived from the kappa-opioid receptor)[40] in a Cre-dependent manner (Extended Data Fig. 8a,b). These mice were first trained in the AAA task (Extended Data Fig. 8c), and subsequently tested in a session in which their Fezf2^{BLa} neurons were inhibited by systemic application of salvinorin B (SALB), the agonist of KORD[40]. Remarkably, inhibition of Fezf2^{BLa} neurons markedly and reversibly reduced the licking responses induced by CS_R, but did not affect the subsequent licking triggered by US_R in the same trial (Extended Data Fig. 8d,f,g). In a similar manner, the inhibition markedly and reversibly reduced the running responses induced by CS_P, but did not affect the subsequent running triggered by US_P in the same trial (Extended Data Fig. 8e,i,j). Control experiments confirmed that vehicle treatment, or treating animals with SALB alone did not affect animals' behavior in the AAA task (Extended Data Fig. 8d–k).

These results indicate that Fezf2^{BLa} neurons are essential for anticipating, or motivating actions to pursue the goal of obtaining reward or avoiding punishment, but are dispensable for generating the specific movements (licking and running) per se that let animals reach such goals.

Fezf2$^{BLa\rightarrow NAc}$ and Fezf2$^{BLa\rightarrow OT}$ have essential behavioral roles. To determine whether Fezf2$^{BLa\rightarrow NAc}$ and Fezf2$^{BLa\rightarrow OT}$ neurons are differentially required for learning or expressing valence-specific behaviors, we sought to selectively and transiently inhibit each of these populations during and after learning in the AAA task. To achieve this goal, we expressed the light-sensitive *Guillardia theta* anion-conducting channelrhodopsin 2 (GtACR2)[41,42] selectively in Fezf2$^{BLa\rightarrow NAc}$ or Fezf2$^{BLa\rightarrow OT}$ neurons using the intersectional viral strategy described above (Extended Data Figs. 5d–i and 7). Specifically, we bilaterally injected the NAc or OT of *Fezf2-Flp* mice with the AAVrg expressing Cre in a Flp-dependent manner, and injected the BLa of the same mice with an AAV expressing GtACR2, or GFP (as a control), in a Cre-dependent manner (Extended Data Fig. 9a–d). Optical fibers were implanted in the BLa above the infected areas for photostimulation (Supplementary Fig. 6a,b). These mice were trained in the AAA task and received photostimulation in the BLa in a time window covering CS and US presentations in each trial throughout the training (Extended Data Fig. 9e,f). The mice were subsequently given additional training in the absence of photostimulation (to allow the GtACR2 and GFP groups to reach equal performance), followed by a test session ('after learning') in which the photostimulation was delivered in a subset of randomly chosen trials (Extended Data Fig. 9f and Methods).

We found that, in mice where Fezf2$^{BLa\rightarrow NAc}$ neurons were targeted, the photostimulation during learning caused a decrease in performance in punishment trials, but not in reward trials in the GtACR2 group compared with the GFP group (Fig. 7a,b). By contrast, in mice where Fezf2$^{BLa\rightarrow OT}$ neurons were targeted, the photostimulation during learning caused a decrease in performance in reward trials, but not in punishment trials in the GtACR2 group compared with the GFP group (Fig. 7c,d). Furthermore, in the 'after learning' test session, photostimulation of Fezf2$^{BLa\rightarrow NAc}$ neurons in the GtACR2 group caused a decrease in anticipatory running in punishment trials, but did not affect anticipatory licking in reward trials (Fig. 7e,g), whereas photostimulation of Fezf2$^{BLa\rightarrow OT}$ neurons in the GtACR2 group caused a decrease in anticipatory licking in reward trials, but did not affect anticipatory running in punishment trials (Fig. 7f,h). The photostimulation did not affect the behavioral responses in the GFP groups (Fig. 7e–h).

Together, these results indicate that Fezf2$^{BLa\rightarrow NAc}$ neurons are selectively required for learning and expression of punishment-avoidance actions, while the Fezf2$^{BLa\rightarrow OT}$ neurons are selectively required for learning and expression of reward-seeking responses.

Fezf2$^{BLa\rightarrow NAc}$ and Fezf2$^{BLa\rightarrow OT}$ differently instruct learning. To further understand how the signals from Fezf2$^{BLa\rightarrow NAc}$ and Fezf2$^{BLa\rightarrow OT}$ neurons might contribute to valence-specific behaviors, we tested the effects of activating these neurons with optogenetics. For this purpose, we again used the intersectional strategy to express ChR2, or GFP (as a control), selectively in Fezf2$^{BLa\rightarrow NAc}$ or Fezf2$^{BLa\rightarrow OT}$ neurons, followed by optical fiber implantation in the BLa for photostimulation (Extended Data Fig. 9g–j and Supplementary Fig. 6c–i). We found that brief photostimulation of either Fezf2$^{BLa\rightarrow NAc}$ (Extended Data Fig. 9k–m) or Fezf2$^{BLa\rightarrow OT}$ (Extended Data Fig. 9n–p) neurons in the ChR2 mice, but not GFP mice, reliably and drastically induced pupil enlargement. This result suggests that activities in either population promote affective or motivational arousal, a crucial factor determining learning and performance in motivated behaviors[43–45].

Fig. 6 | Fezf2$^{BLa\rightarrow NAc}$ and Fezf2$^{BLa\rightarrow OT}$ neurons receive distinct sets of monosynaptic inputs. a, A schematic of the approach. **b**, A confocal image showing injection location in the NAc indicated by fluorescent beads (arrow). **c**, Confocal images of the BLa showing the Fezf2$^{BLa\rightarrow NAc}$ neurons infected with the starter virus (left) and the rabies virus (middle) and the colocalization (right). **d**, Images showing the major areas labeled by the rabies virus. **e**, A schematic of the approach. **f**, A confocal image showing injection location indicated by fluorescent beads (arrow). **g**, Confocal images of the BLa showing the Fezf2$^{BLa\rightarrow OT}$ neurons infected with the starter virus (left) and the rabies virus (middle) and the colocalization (right). **h**, Images showing the major areas labeled by the rabies virus. **i**, Whole-brain quantification of rabies-labeled areas ($n = 8$ mice for each pathway; Friedman test with Dunn's post hoc test, F-stat 304.3, $P < 0.0001$; $^{*}P < 0.05$, $^{**}P < 0.01$, $^{***}P < 0.001$, $^{****}P < 0.0001$; P values between Fezf2$^{BLa\rightarrow NAc}$ and Fezf2$^{BLa\rightarrow OT}$: PL, 0.2458; IL, 0.0932; Mop, 0.1805; SI, 0.5438; PIR, <0.0001; CoA, 0.0029; ACC, 0.6361; PVT: 0.0065; MD, 0.5320; CM, 0.3719; RE: 0.0549; BL, 0.9431; LA, 0.3173; CeA, 0.1291; ENT, 0.2421; AuD, 0.1080; vHC, 0.8723; MGv, <0.0001; MGd, 0.0727; MGm, 0.7210; PIL, 0.1268; PR, 0.0055; CLI, 0.0038; MRN, 0.0031). Data are presented as the mean ± s.e.m. PL, prelimbic area; IL, infralimbic area; MOp, primary motor area; SI, substantia innominata; ACC, anterior cingulate cortex; MD, mediodorsal nucleus of the thalamus; CM, central medial nucleus of the thalamus; RE, nucleus of reuniens; BL, basolateral amygdalar nucleus; CeA, central amygdalar nucleus; AuD, auditory areas; vHC, ventral hippocampus; MGd, medial geniculate complex, dorsal part; MGm, medial geniculate complex, medial part; CLI, central linear nucleus raphe; MRN, midbrain reticular nucleus.

To probe if the arousal is related to perception of positive or negative valence, we tested these mice in a real-time place preference or aversion (RTPP/RTPA) test, in which the photostimulation was contingent on entering one side of a chamber containing two compartments. In stark contrast, stimulating Fezf2$^{BLa\rightarrow NAc}$ neurons caused avoidance, whereas stimulating Fezf2$^{BLa\rightarrow OT}$ neurons induced prefer-

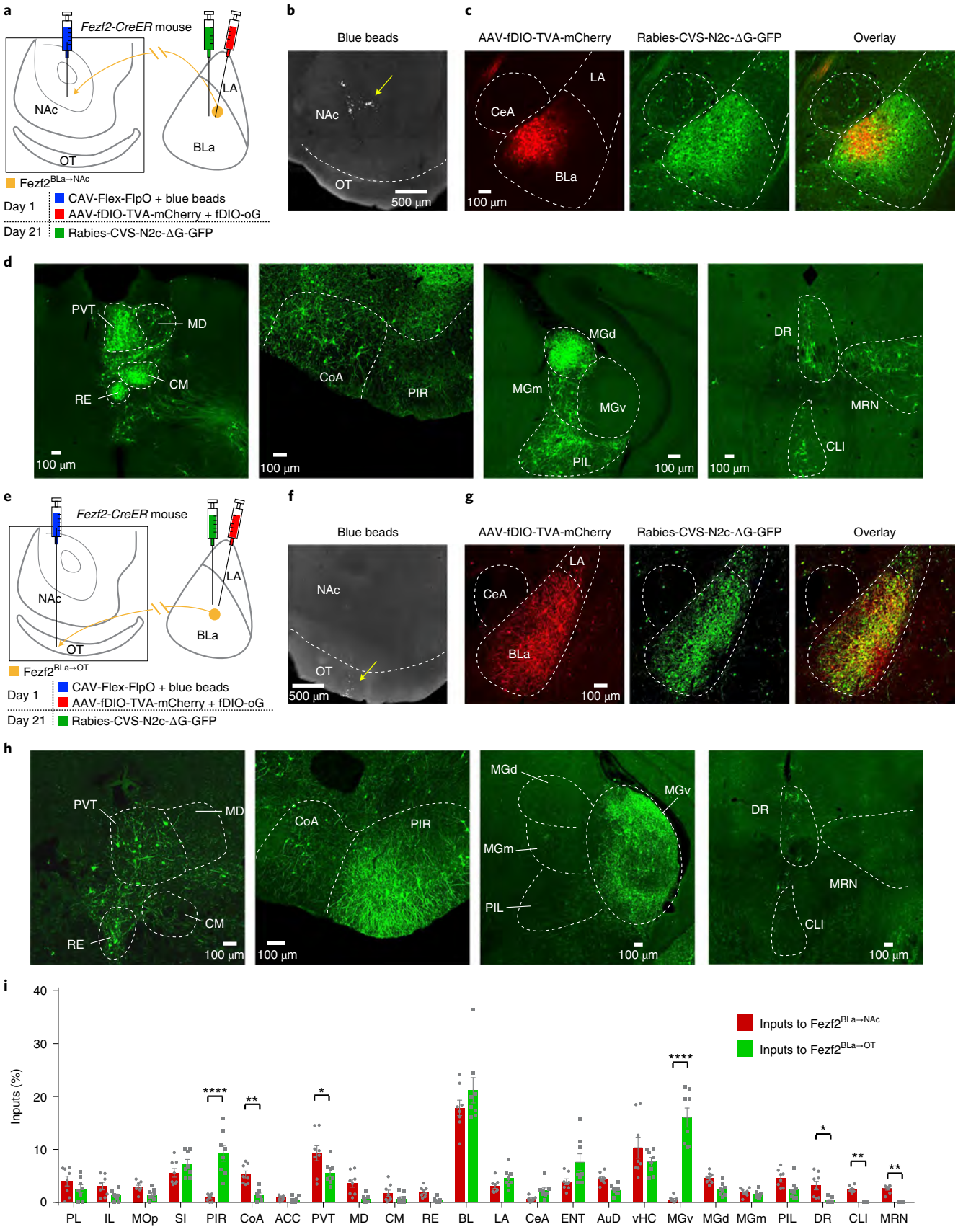

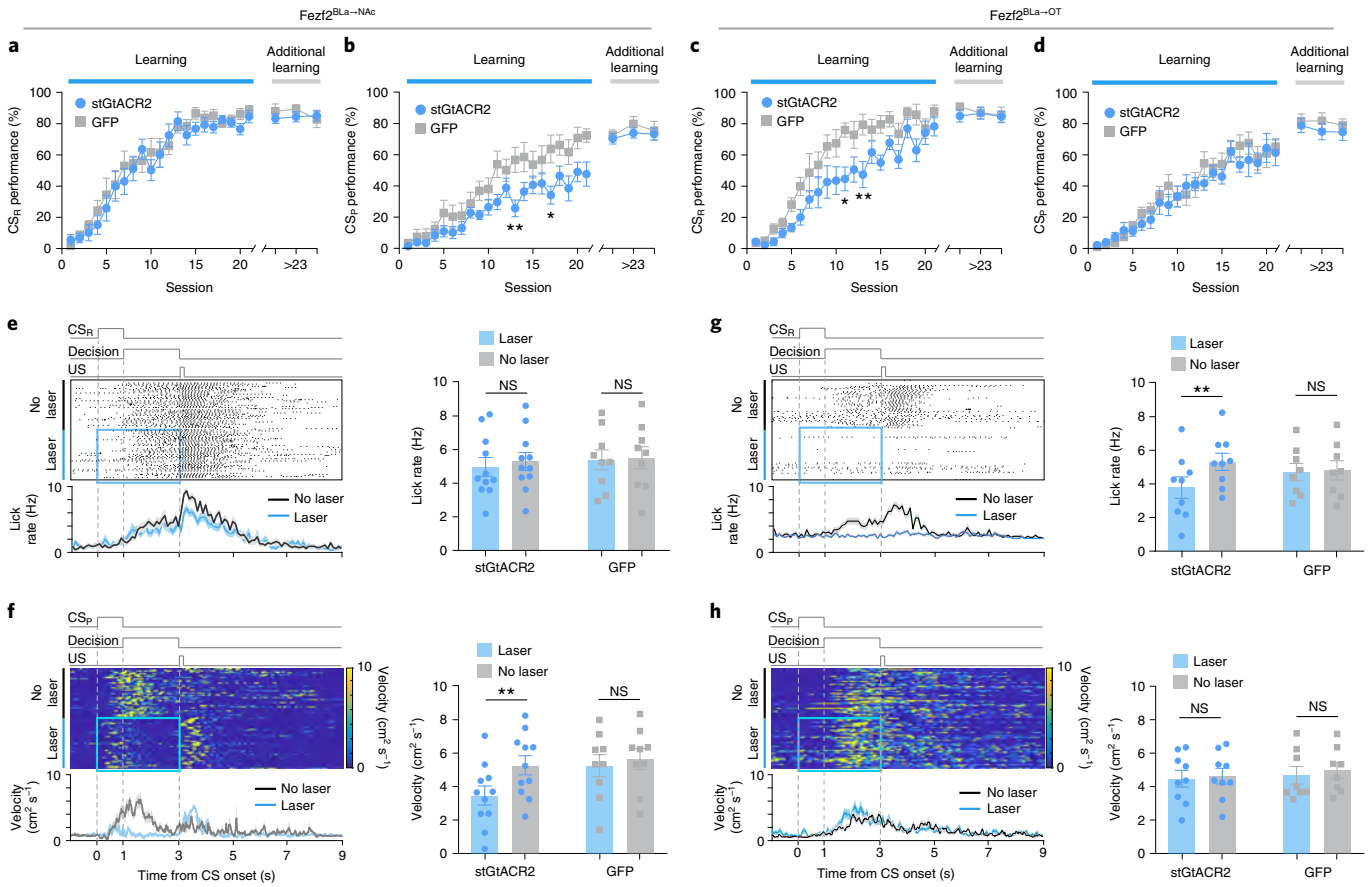

Fig. 7 | Fezf2$^{BLa→NAc}$ and Fezf2$^{BLa→OT}$ are differentially required for approach or avoidance. a–d, During learning. **a**, Performance of mice having Fezf2$^{BLa→NAc}$ neurons infected (GtACR2, $n=11$; GFP, $n=9$), in reward trials with laser (left; $F(1, 378)=3.34$, $P=0.069$), and without laser (right; $F(1, 54)=0.5765$, $P=0.451$). **b**, Performance of the mice in **a** in punishment trials with laser (left; $F(1, 378)=63.08$, $P<0.0001$; $^{*}P=0.0126$, $^{**}P=0.0071$), and without laser (right; $F(1, 54)=1.024$, $P=0.316$). **c**, **d**, Same as **a** and **b**, except that Fezf2$^{BLa→OT}$ neurons were infected (GtACR2, $n=9$; GFP, $n=8$). **c**, With laser (left; $F(1, 315)=65.11$, $P<0.0001$; $^{*}P=0.013$, $^{**}P=0.009$), and without laser (right; $F(1, 45)=0.5992$, $P=0.443$). **d**, With laser (left), $F(1, 315)=2.863$, $P=0.092$. Without laser (right), $F(1, 48)=0.5015$, $P=0.4823$. **e**–**h**, After learning. **e**,**f**, Mice having Fezf2$^{BLa→NAc}$ neurons infected (soma-targeted (st) GtACR2, $n=11$; GFP, $n=9$). **e**, Left, raster (upper) and average (lower) plots of licking behavior of a mouse in reward trials. Laser stimulation period is indicated by a blue box. Right, lick rate during decision window ($F(1, 18)=0.3164$, $P=0.58$; stGtACR2, $P=0.3530$; GFP, $P=0.8796$). **f**, Left, raster (upper) and average (lower) plots of running behavior of a mouse in punishment trials. Laser stimulation period is indicated by a blue box. Right, running velocity during decision window ($F(1, 18)=11.43$, $P=0.0033$; stGtACR2, $^{**}P=0.0013$; GFP, $P=0.661$;). **g**,**h**, Same as **e** and **f**, except that Fezf2$^{BLa→OT}$ neurons were infected (stGtACR2, $n=9$; GFP, $n=8$). **g**, $F(1,15)=7.287$, $P=0.0165$; stGtACR2, $^{**}P=0.0015$; GFP, $P=0.9562$. **h**, $F(1, 15)=3.63$, $P=0.076$; stGtACR2, $P=0.5779$; GFP, $P=0.2042$. Statistics were from two-way ANOVA with repeated measures followed by Bonferroni's multiple-comparisons test. Data are presented as the mean ± s.e.m.

ence to the side paired with the stimulation (Fig. 8a–d). These results suggest that the activities in Fezf2$^{BLa→NAc}$ and Fezf2$^{BLa→OT}$ neurons promote arousal by signaling negative and positive valence, respectively.

If Fezf2$^{BLa→NAc}$ and Fezf2$^{BLa→OT}$ neurons are crucial for representing and conveying negative-valence and positive-valence information, respectively, activation of these neurons should differentially instruct valence-specific learning. To test this hypothesis, we trained the mice in which Fezf2$^{BLa→NAc}$ or Fezf2$^{BLa→OT}$ neurons were targeted in a two-port choice task, where poking one port (the active port) resulted in photostimulation of Fezf2$^{BLa→NAc}$ or Fezf2$^{BLa→OT}$ neurons, whereas poking the other (the inactive port) resulted in nothing (Fig. 8e). The mice in which Fezf2$^{BLa→NAc}$ neurons were targeted (including the ChR2 and GFP groups) did not make much effort to poke into either the active or the inactive port (Fig. 8f–h). However, the mice in the ChR2 group in which Fezf2$^{BLa→OT}$ neurons were targeted quickly learned to poke the active port while ignoring the inactive one, vigorously performing self-stimulation (Fig. 8i,j). Moreover, in a reversal test conducted 24 h later, the mice persisted in choosing the initial active port even if the port had become inactive (Fig. 8k).

Next, we trained the mice in an optically driven active avoidance task. We took advantage of the design for active avoidance in the AAA task (Fig. 3a), but substituted photostimulation of Fezf2$^{BLa→NAc}$ or Fezf2$^{BLa→OT}$ neurons for air puff as a potential negative reinforcer (Fig. 8l). Remarkably, photostimulation of Fezf2$^{BLa→NAc}$ neurons in the ChR2 group was sufficient to instruct learning, such that the mice acquired running response to CS and thus successfully avoided the photostimulation, in a manner similar to avoiding the air puff in the AAA task (Fig. 8m,n). Photostimulation of Fezf2$^{BLa→OT}$ neurons failed to support such learning (Fig. 8o,p). Control experiments showed that photostimulation in the GFP groups did not affect animals' behavior in all the tests performed (Fig. 8 and Extended Data Fig. 9k–p). Importantly, essentially no PPP1R1B^{+} neurons could be found in the BLa locations where we targeted the *Fezf2*$^{+}$ neurons (Supplementary Fig. 6c–h).

In a separate set of experiments, we repeated all the above-described photostimulation experiments based on ChR2, with the exception that the photostimulation was delivered to the NAc or OT, to stimulate the axon terminals originating from Fezf2^{BLa} neurons (Extended Data Fig. 10 and Supplementary Fig. 7).

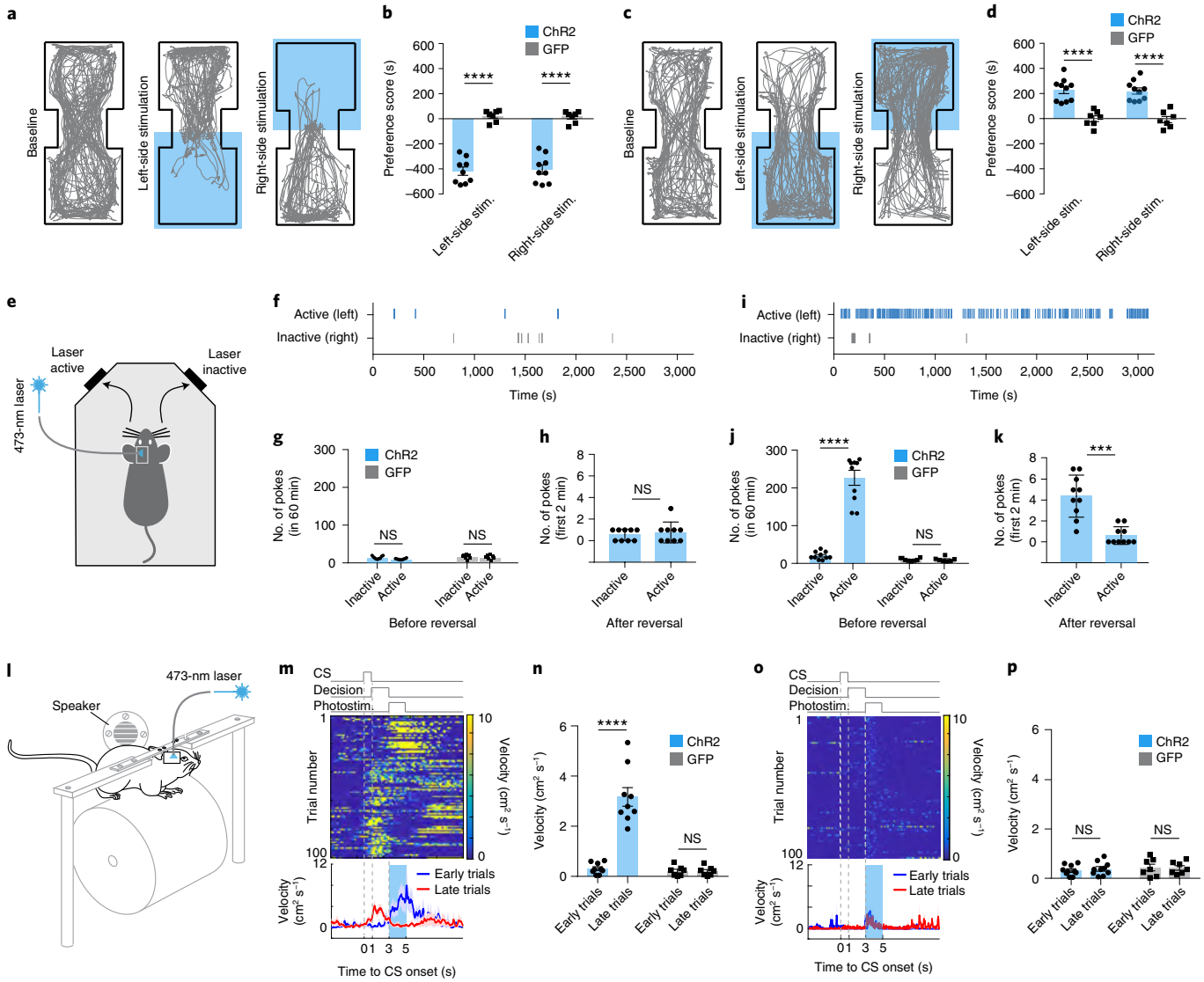

Fig. 8 | Fezf2$^{BLa\rightarrow NAc}$ and Fezf2$^{BLa\rightarrow OT}$ neurons differentially instruct learning. a, Movement trajectory of a mouse at baseline (left), or in a situation whereby entering the left (middle) or right (right) side of the chamber triggered photoactivation of Fezf2$^{BLa\rightarrow NAc}$ neurons. **b**, Quantification of behavior as shown in **a**, for mice in which ChR2 ($n=9$) or GFP ($n=7$) was expressed in Fezf2$^{BLa\rightarrow NAc}$ neurons ($F(1, 28)=202.5$, $P<0.0001$; $^{****}P<0.0001$; NS, $P>0.05$; two-way ANOVA followed by Bonferroni's multiple-comparisons test). **c**,**d**, Same as **a** and **b**, respectively, except that Fezf2$^{BLa\rightarrow OT}$ neurons were targeted (ChR2, $n=10$; GFP, $n=7$; $F(1, 30)=73.05$, $P<0.0001$; $^{****}P<0.0001$, NS, $P>0.05$; two-way ANOVA followed by Bonferroni's multiple-comparisons test). **e**, A schematic of the approach. **f**, Raster plot of nose-poking events at active (with laser) or inactive (without laser) port, for a mouse in which ChR2 was expressed in Fezf2$^{BLa\rightarrow NAc}$ neurons. **g**, Quantification of nose-poking events in a 60-min session for mice in which ChR2 ($n=9$) or GFP ($n=7$) was expressed in Fezf2$^{BLa\rightarrow NAc}$ neurons ($F(1, 28)=1.09$, $P=0.3$; NS, $P>0.05$; two-way ANOVA). **h**, Quantification of nose-poking events of the ChR2 mice in **g**, in the first 2 min of the reversal test, in which the active and inactive ports were switched ($P>0.99$; Mann–Whitney test, $U=38$). **i**, Same as **f**, except that ChR2 was expressed in Fezf2$^{BLa\rightarrow OT}$ neurons. **j**, Same as **g**, except that Fezf2$^{BLa\rightarrow OT}$ neurons were targeted (ChR2, $n=10$; GFP, $n=7$; $F(1, 30)=70.53$, $P<0.0001$; $^{****}P<0.0001$, NS, $P>0.05$; two-way ANOVA followed by Bonferroni's multiple-comparisons test). **k**, Same as **h**, except that ChR2 was expressed in Fezf2$^{BLa\rightarrow OT}$ neurons ($^{***}P=0.0001$; Mann–Whitney test, $U=4$). **l**, A schematic of the approach. **m**, Top, trial-by-trial heat maps of running velocity for an example mouse in the active avoidance task; bottom, average running velocity of the mouse in early (first ten trials) and late (last ten trials) trials. **n**, Quantification of running velocity during the decision window in early (first ten) and late (last ten) trials (ChR2 mice, $n=9$, GFP mice, $n=7$; $F(1, 28)=42.3$, $P<0.0001$; $^{****}P<0.0001$, NS, $P>0.05$; two-way ANOVA followed by Bonferroni's multiple-comparisons test). **o**,**p**, Same as **m** and **n**, respectively, except that Fezf2$^{BLa\rightarrow OT}$ neurons were targeted (ChR2 mice, $n=10$, GFP mice, $n=7$; $F(1, 30)=0.24$, $P=0.63$; NS, $P>0.05$; two-way ANOVA). Data are presented as the mean ± s.e.m.

The results from these experiments, which targeted Fezf2$^{BLa\rightarrow NAc}$ and Fezf2$^{BLa\rightarrow OT}$ axon terminals, fully recapitulated those from the experiments described above that targeted the cell bodies of the respective neuronal populations (Extended Data Fig. 9g–p, Fig. 8 and Supplementary Fig. 6c–i).

Together, these results indicate that the activities in Fezf2$^{BLa\rightarrow NAc}$ neurons serve as a negative reinforcer to instruct avoidance learning, while activities in Fezf2$^{BLa\rightarrow OT}$ neurons serve as a positive reinforcer that supports self-stimulation and drives formation of appetitive memories.

$Fezf2^{BLa \rightarrow mPFC}$ and $Fezf2^{BLa \rightarrow LS}$ have different functions. Finally, as $Fezf2^{BLa}$ neurons also send projections to the mPFC and LS (Extended Data Fig. 5a–i), we examined the effect of optogenetic activation of these projections in the RTPP/RTPA test (Supplementary Fig. 8), using the same strategy as described above (Extended Data Fig. 10a–d,k–n). Activation of either the $Fezf2^{BLa \rightarrow mPFC}$ (Supplementary Fig. 8a–e) or the $Fezf2^{BLa \rightarrow LS}$ (Supplementary Fig. 8f–j) pathway did not induce any obvious behavioral effect in this test. Future research will need to elucidate the potential functions of these pathways.

Discussion

Valence-specific neurons in the BLA. Through imaging $Fezf2^{BLa}$ neurons during behavior, we discovered two functionally distinct populations, with one (PVNs) being excited by an appetitive but not aversive US, and the other (NVNs) excited by an aversive but not appetitive US. These PVNs and NVNs underwent plasticity during learning, such that they acquired excitatory responses to the CS entrained by appetitive or aversive US, respectively, after learning. As a result, the number of $Fezf2^{BLa}$ neurons excited by either of the CS increased with learning. These results show that the BLA contains valence-specific neurons and provide, to our knowledge, for the first time direct in vivo evidence that CS acquire the ability to activate valence-specific BLA neurons through learning.

The CS responses in PVNs and NVNs preceded and were coupled with reward-seeking and punishment-avoidance actions, respectively. At the population level, the CS responses of $Fezf2^{BLa}$ neurons predicted valence-specific behaviors on a trial-by-trial basis. This tight relationship after, but not before learning suggests an important role of these neurons in guiding or promoting goal-directed behaviors acquired through experience. Indeed, chemogenetic inhibition of these neurons prevented the CS-induced reward seeking and punishment avoidance in well-trained animals. Notably, this manipulation did not affect the very same action (licking or running) evoked by a US immediately following the CS. This remarkable specificity indicates that $Fezf2^{BLa}$ neurons were not required for generating the specific movements (licking and running) that ultimately let animals reach their goals; rather, they were required for anticipating or motivating such actions. We propose that $Fezf2^{BLa}$ neurons, in particular the PVNs and NVNs, play a critical role in generating positive and negative motivations or saliences, respectively, that underlie valence-specific behaviors.

Distinct BLa-ventral striatal circuits for opposing valences. Through circuit mapping, pathway-specific fiber photometry and optogenetics, we found that $Fezf2^{BLa}$ neurons had two major targets—the NAc and the OT— both of which belong to the ventral striatum[30]. Furthermore, the response properties and functions of $Fezf2^{BLa \rightarrow NAc}$ and $Fezf2^{BLa \rightarrow OT}$ neurons suggest that they are NVNs and PVNs, respectively.

The in vivo properties and behavioral functions of $Fezf2^{BLa \rightarrow NAc}$ neurons that we describe here provide a mechanistic explanation for previous findings that the BLA → NAc pathway is involved in aversive behaviors[5,6,46,47]. Of note, it has also been shown that the BLA → NAc pathway plays an important role in reward-related behaviors[10–12,48]. These observations indicate that NAc-projecting BLA neurons are functionally heterogeneous. While $Fezf2^{BLa \rightarrow NAc}$ neurons represent negative valence and are essential for negative reinforcement, other NAc-projecting BLA neurons, yet to be identified, likely have opposing or different functions.

The properties and functions of the BLa → OT pathway have not been described previously. It has been shown that the OT plays an important role in reward-related behaviors[31,49–52]. Our results from $Fezf2^{BLa \rightarrow OT}$ neurons provide, to the best of our knowledge, the first evidence that positive valence or motivation information is conveyed from the BLa to the OT, and establish a critical role for the OT in the BLA valence-specific circuits.

It is worth noting that our anatomical and functional circuit-mapping experiments suggest that, although $Fezf2^{BLa \rightarrow NAc}$ and $Fezf2^{BLa \rightarrow OT}$ neurons preferentially project to the NAc and OT, respectively, they do send collaterals to the other targets. These collaterals may play an important role in coordinating the activities across brain areas during valence-specific behaviors.

A circuit framework for valence-specific behaviors. We show that $Fezf2^{BLa \rightarrow NAc}$ and $Fezf2^{BLa \rightarrow OT}$ neurons receive distinct sets of monosynaptic inputs. This result suggests that the two classes, and hence the NVNs and PVNs in the BLA, are 'hardwired' in distinct input–output circuits. These circuits may represent the key actors that play the previously established roles of the BLA in encoding, learning and expressing valence-specific behaviors[2,3,48,53].

The ventral striatum has long been considered an interface between limbic and motor areas[30,31,54]. Future studies need to elucidate how the negative and positive motivational signals from BLA NVNs and PVNs, respectively, are further transformed in the NAc and OT for guiding valence-specific behaviors. It will also be important to determine how neurons in the distinct input structures interact with the NVNs and PVNs, to give rise to the valence-specific motivational signals therein.

Online content

Any methods, additional references, Nature Research reporting summaries, source data, extended data, supplementary information, acknowledgements, peer review information; details of author contributions and competing interests; and statements of data and code availability are available at https://doi.org/10.1038/s41593-021-00927-0.

Received: 31 May 2020; Accepted: 25 August 2021;
Published online: 18 October 2021

References

1. Gore, F. et al. Neural representations of unconditioned stimuli in basolateral amygdala mediate innate and learned responses. *Cell* **162**, 134–145 (2015).
2. O'Neill, P. K., Gore, F. & Salzman, C. D. Basolateral amygdala circuitry in positive and negative valence. *Curr. Opin. Neurobiol.* **49**, 175–183 (2018).
3. Pignatelli, M. & Beyeler, A. Valence coding in amygdala circuits. *Curr. Opin. Behav. Sci.* **26**, 97–106 (2019).
4. Redondo, R. L. et al. Bidirectional switch of the valence associated with a hippocampal contextual memory engram. *Nature* **513**, 426–430 (2014).
5. Kim, J., Pignatelli, M., Xu, S., Itohara, S. & Tonegawa, S. Antagonistic negative and positive neurons of the basolateral amygdala. *Nat. Neurosci.* **19**, 1636–1646 (2016).
6. Shen, C. J. et al. Cannabinoid CB1 receptors in the amygdalar cholecystokinin glutamatergic afferents to nucleus accumbens modulate depressive-like behavior. *Nat. Med.* **25**, 337–349 (2019).
7. Zhang, X., Kim, J. & Tonegawa, S. Amygdala reward neurons form and store fear extinction memory. *Neuron* **105**, 1077–1093 (2020).
8. Fusi, S., Miller, E. K. & Rigotti, M. Why neurons mix: high dimensionality for higher cognition. *Curr. Opin. Neurobiol.* **37**, 66–74 (2016).
9. Kyriazi, P., Headley, D. B. & Pare, D. Multidimensional coding by basolateral amygdala neurons. *Neuron* **99**, 1315–1328 (2018).
10. Stuber, G. D. et al. Excitatory transmission from the amygdala to nucleus accumbens facilitates reward seeking. *Nature* **475**, 377–380 (2011).
11. Namburi, P. et al. A circuit mechanism for differentiating positive and negative associations. *Nature* **520**, 675–678 (2015).
12. Britt, J. P. et al. Synaptic and behavioral profile of multiple glutamatergic inputs to the nucleus accumbens. *Neuron* **76**, 790–803 (2012).
13. Beyeler, A. et al. Organization of valence-encoding and projection-defi ed neurons in the basolateral amygdala. *Cell Rep.* **22**, 905–918 (2018).
14. Beyeler, A. et al. Divergent routing of positive and negative information from the amygdala during memory retrieval. *Neuron* **90**, 348–361 (2016).
15. Lodato, S. et al. Gene co-regulation by *Fezf2* selects neurotransmitter identity and connectivity of corticospinal neurons. *Nat. Neurosci.* **17**, 1046–1054 (2014).

16. Tantirigama, M. L., Oswald, M. J., Duynstee, C., Hughes, S. M. & Empson, R. M. Expression of the developmental transcription factor Fezf2 identifies a distinct subpopulation of layer 5 intratelencephalic-projection neurons in mature mouse motor cortex. *J. Neurosci.* **34**, 4303–4308 (2014).
17. Harris, K. D. & Shepherd, G. M. The neocortical circuit: themes and variations. *Nat. Neurosci.* **18**, 170–181 (2015).
18. Hirata-Fukae, C. & Hirata, T. The zinc fi ger gene *Fezf2* is required for the development of excitatory neurons in the basolateral complex of the amygdala. *Dev. Dyn.* **243**, 1030–1036 (2014).
19. Carlsen, J. & Heimer, L. The basolateral amygdaloid complex as a cortical-like structure. *Brain Res.* **441**, 377–380 (1988).
20. Matho, K. S. et al. Genetic dissection of glutamatergic neuron subpopulations and developmental trajectories in the cerebral cortex. Preprint at *bioRxiv* https://www.biorxiv.org/content/10.1101/2020.04.22.054064v1; *Nature*, in press (2021).
21. Madisen, L. et al. A robust and high-throughput Cre reporting and characterization system for the whole mouse brain. *Nat. Neurosci.* **13**, 133–140 (2010).
22. He, M. et al. Cell-type-based analysis of microRNA profiles in the mouse brain. *Neuron* **73**, 35–48 (2012).
23. McDonald, A. J., Muller, J. F. & Mascagni, F. GABAergic innervation of alpha type II calcium/calmodulin-dependent protein kinase immunoreactive pyramidal neurons in the rat basolateral amygdala. *J. Comp. Neurol.* **446**, 199–218 (2002).
24. Chen, T. W. et al. Ultrasensitive fluorescent proteins for imaging neuronal activity. *Nature* **499**, 295–300 (2013).
25. Kim, J., Zhang, X., Muralidhar, S., LeBlanc, S. A. & Tonegawa, S. Basolateral to central amygdala neural circuits for appetitive behaviors. *Neuron* **93**, 1464–1479 (2017).
26. Fenno, L. E. et al. Targeting cells with single vectors using multiple-feature Boolean logic. *Nat. Methods* **11**, 763–772 (2014).
27. Gallistel, C. R., Fairhurst, S. & Balsam, P. The learning curve: implications of a quantitative analysis. *Proc. Natl Acad. Sci. USA* **101**, 13124–13131 (2004).
28. Paton, J. J., Belova, M. A., Morrison, S. E. & Salzman, C. D. The primate amygdala represents the positive and negative value of visual stimuli during learning. *Nature* **439**, 865–870 (2006).
29. Cunningham, J. P. & Yu, B. M. Dimensionality reduction for large-scale neural recordings. *Nat. Neurosci.* **17**, 1500–1509 (2014).
30. de Olmos, J. S. & Heimer, L. The concepts of the ventral striatopallidal system and extended amygdala. *Ann. N. Y. Acad. Sci.* **877**, 1–32 (1999).
31. Wesson, D. W. & Wilson, D. A. Sniffing out the contributions of the olfactory tubercle to the sense of smell: hedonics, sensory integration, and more? *Neurosci. Biobehav. Rev.* **35**, 655–668 (2011).
32. Petreanu, L., Mao, T., Sternson, S. M. & Svoboda, K. The subcellular organization of neocortical excitatory connections. *Nature* **457**, 1142–1145 (2009).
33. Yu, K., Garcia da Silva, P., Albeanu, D. F. & Li, B. Central amygdala somatostatin neurons gate passive and active defensive behaviors. *J. Neurosci.* **36**, 6488–6496 (2016).
34. Xiao, X. et al. A genetically defi ed compartmentalized striatal direct pathway for negative reinforcement. *Cell* **183**, 211–227 (2020).
35. Schwarz, L. A. et al. Viral-genetic tracing of the input–output organization of a central noradrenaline circuit. *Nature* **524**, 88–92 (2015).
36. Reardon, T. R. et al. Rabies virus CVS-N2c$^{\Delta G}$ strain enhances retrograde synaptic transfer and neuronal viability. *Neuron* **89**, 711–724 (2016).
37. Schiff, H. C. et al. An insula-central amygdala circuit for guiding tastant-reinforced choice behavior. *J. Neurosci.* **38**, 1418–1429 (2018).
38. Stephenson-Jones, M. et al. Opposing contributions of GABAergic and glutamatergic ventral pallidal neurons to motivational behaviors. *Neuron* **105**, 921–933 (2020).
39. Stephenson-Jones, M. et al. A basal ganglia circuit for evaluating action outcomes. *Nature* **539**, 289–293 (2016).
40. Vardy, E. et al. A new DREADD facilitates the multiplexed chemogenetic interrogation of behavior. *Neuron* **86**, 936–946 (2015).
41. Govorunova, E. G., Sineshchekov, O. A., Janz, R., Liu, X. & Spudich, J. L. NEUROSCIENCE. Natural light-gated anion channels: a family of microbial rhodopsins for advanced optogenetics. *Science* **349**, 647–650 (2015).
42. Mahn, M. et al. High-effici cy optogenetic silencing with soma-targeted anion-conducting channelrhodopsins. *Nat. Commun.* **9**, 4125 (2018).
43. Lang, P. J. & Davis, M. Emotion, motivation, and the brain: reflex foundations in animal and human research. *Prog. Brain Res.* **156**, 3–29 (2006).
44. Russell, J. A. A circumplex model of affect. *J. Pers. Soc. Psychol.* **39**, 1161–1178 (1980).
45. Tye, K. M. Neural circuit motifs in valence processing. *Neuron* **100**, 436–452 (2018).
46. Choi, J. S., Cain, C. K. & LeDoux, J. E. The role of amygdala nuclei in the expression of auditory signaled two-way active avoidance in rats. *Learn Mem.* **17**, 139–147 (2010).
47. Ramirez, F., Moscarello, J. M., LeDoux, J. E. & Sears, R. M. Active avoidance requires a serial basal amygdala to nucleus accumbens shell circuit. *J. Neurosci.* **35**, 3470–3477 (2015).
48. Janak, P. H. & Tye, K. M. From circuits to behaviour in the amygdala. *Nature* **517**, 284–292 (2015).
49. Fitzgerald, B. J., Richardson, K. & Wesson, D. W. Olfactory tubercle stimulation alters odor preference behavior and recruits forebrain reward and motivational centers. *Front. Behav. Neurosci.* **8**, 81 (2014).
50. Ikemoto, S. Involvement of the olfactory tubercle in cocaine reward: intracranial self-administration studies. *J. Neurosci.* **23**, 9305–9311 (2003).
51. Ikemoto, S., Qin, M. & Liu, Z. H. The functional divide for primary reinforcement of d-amphetamine lies between the medial and lateral ventral striatum: is the division of the accumbens core, shell, and olfactory tubercle valid? *J. Neurosci.* **25**, 5061–5065 (2005).
52. Zhang, Z. et al. Activation of the dopaminergic pathway from VTA to the medial olfactory tubercle generates odor-preference and reward. *Elife* **6**, e25423 (2017).
53. Grundemann, J. & Luthi, A. Ensemble coding in amygdala circuits for associative learning. *Curr. Opin. Neurobiol.* **35**, 200–206 (2015).
54. Mogenson, G. J., Jones, D. L. & Yim, C. Y. From motivation to action: functional interface between the limbic system and the motor system. *Prog. Neurobiol.* **14**, 69–97 (1980).

Methods

Animals. Male and female mice aged 2–4 months were used in all the experiments. Mice were housed under a 12-h light–dark cycle (7.00 to 19.00 light) in groups of 2–4 animals, with a room temperature (RT) of 22 °C and humidity of 50%. Food and water were available ad libitum before behavioral training. All behavioral experiments were performed during the light cycle. Littermates were randomly assigned to different groups before experiments. All mice were bred onto a C57BL/6J background. All experimental procedures were approved by the Institutional Animal Care and Use Committee of Cold Spring Harbor Laboratory (CSHL) and performed in accordance with the US National Institutes of Health (NIH) guidelines.

The *Fezf2-CreER* or *Fezf2-Flp* knock-in mouse driver line, in which the expression of the inducible Cre recombinase (CreER) or *Flp*, respectively, is driven by the endogenous *Fezf2* promoter, was generated as previously described[55,56]. A gene-targeting vector for *Fezf2-CreER* or *Flp* was generated using a PCR-based cloning approach[55] to insert an in-frame *2A-CreER* or *2A-Flp* coding cassette, respectively, immediately before the STOP codon of the *Fezf2* gene[20]. The targeting vector was linearized and transfected into C57BL/6 embryonic stem cells. G418-resistant embryonic stem cell clones were first screened by PCR and then confirmed by Southern blotting using probes against the 5′ and 3′ homology arms of the targeted site. The *Ai14* reporter mice[21] were purchased from Jackson Laboratory (007908). The *H2B-GFP* (*Rosa26-stop^{loxP}-H2B-GFP*) reporter mouse line[22] was generated by the laboratory of Z.J.H. at CSHL.

Viral vectors. The rAAV5-Ef1a-DIO-hChR2-eYFP, AAV9-CAG-Flex-GFP and AAV8-hSyn-DIO-KORD-IRES-mCitrine vectors were produced by the University of North Carolina Vector Core Facility. The pAAV-Syn-Flex-GCaMP6f-WPRE-SV40 (100833), AAV-Ef1a-DIO-GCaMP6f-P2A-nls-tdTomato (AAVrg; 51083), pAAV-EF1a-fDIO-Cre (121675-AAVrg), pAAV_hSyn1-SIO-stGtACR2-FusionRed (105677-AAV1), pAAV-hSyn-DIO-EGFP (50457-AAVrg) and pAAV-hSyn-DIO-mCherry (50459-AAVrg) vectors were produced by Addgene. CAV-Flex-FlpO was produced by Montpellier vector platform (Plateforme de Vectorologie de Montpellier). The AAVDJ-CAG-fDIO-oG-WPRE-SV40pA was produced by the Viral Vector Core Facility at Salk Institute. The AAV2/8-Ef1a-fDIO-TVA-mCherry was produced by the laboratory of Z.J.H. at CSHL. The Rbv-CVS-N2c-dG-GFP (the optimized rabies virus)[36] was produced by HHMI Janelia Research Campus. The AAV8-CaMKIIa-FDO-GCaMP6f (Flp-off) virus was produced by the laboratory of K.D. at Stanford University. All viral vectors were aliquoted and stored at −80 °C until use.

Stereotaxic surgery. All surgery was performed under aseptic conditions and body temperature was maintained with a heating pad. Standard surgical procedures were used for stereotaxic injection and GRIN lens or optical fiber implantation, as previously described[57,58]. Briefly, mice were anesthetized with isoflurane (3% at the beginning and 1% for the rest of the surgical procedure), and were positioned in a stereotaxic injection frame and on top of a heating pad maintained at 35 °C. A digital mouse brain atlas was linked to the injection frame to guide the identification and targeting of different brain areas (Angle Two Stereotaxic System, http://myNeuroLab.com). We used the following coordinates for injections or implantations in the BLA: −1.6 mm from bregma, 3.3 mm lateral from the midline and 4.5 mm vertical from the skull surface; the NAc (shell and core): 1.5 mm from bregma, 1.0 mm lateral from the midline and 4.6 mm vertical from the skull surface; the OT: 1.5 mm from bregma, 0.8 mm lateral from the midline and 5.0 mm vertical from the skull surface; mPFC: 1.8 mm from bregma, 0.3 mm lateral from the midline and 3 mm vertical from the skull surface; and the LS: 0.3 mm from bregma, 0.5 mm lateral from the midline and 3 mm vertical from the skull surface.

For virus injection, we made a small cranial window (1–2 mm^2) for each mouse, through which a glass micropipette (tip diameter, ~5 µm) containing viral solution was lowered down to the target. About 0.3 µl of viral solution was delivered with pressure applications (5–20 psi, 5–20 ms at 1 Hz) controlled by a Picrospritzer III (General Valve) and a pulse generator (Agilent). The speed of injection was ~0.1 µl min^{-1} over 10 min. We waited for at least 10 min following the injection before slowly removing the injection pipette. For imaging experiments, we implanted the GRIN lens (diameter, 0.6 mm; length, 6.7 mm; Inscopix) 2 weeks after virus injection. The GRIN lens was carefully implanted 200 µm above the center of the injection using a GRIN lens holder (Inscopix). The speed for lowering the GRIN lens was constant and slow (~100 µm min^{-1}) until the target was reached. We secured the GRIN lens to the skull with C&B-Metabond Quick adhesive luting cement (Parkell Prod), and subsequently mounted a small piece of metal bar on the skull for head fixation. We waited 4 to 6 weeks following GRIN lens implantation before starting the imaging experiments.

For optogenetic experiments, we bilaterally implanted optical fibers (diameter, 200 µm; NA, 0.22) into the BLa, NAc or OT. For fiber photometry experiments, we implanted the optical fiber (diameter, 200 µm; NA, 0.37) into the BLa. For the retrograde tracing of Fezf2^{BLa} neurons with the retrograde tracer CTB, we used the *Fezf2;H2B-GFP* mice and injected the NAc and OT in the same mice with CTB conjugated with either Alexa Fluor 647 or Alexa Fluor 555 (CTB-647 or CTB-555, respectively; Invitrogen, Thermo Fisher Scientific; 0.2 µl, 1 mg ml^{-1} in PBS). The animals were perfused 5 d after CTB injection. For certain viral injection, where indicated, a small amount of blue fluorescent microspheres ('blue beads'; Thermo Fisher, F8805, 2% solids, diluted to 0.1% with PBS) was added to the viral solution at a 1:1 volume-to-volume ratio to mark the injection site for histologic verification.

Tamoxifen induction. All *Fezf2-CreER* mice underwent tamoxifen induction to activate the Cre-dependent expression of genes of interest. Tamoxifen (Sigma-Aldrich, WXBC6404V) was dissolved in corn oil at a concentration of 20 mg ml^{-1}, by constant shaking for 24 h at RT in a container protected from light. Individual aliquots (1 ml each) were stored at 4 °C. Tamoxifen induction was performed via intraperitoneal injections at a dose of 0.1 mg per gram of body weight, once every 2 d for three times. For virally driven gene expression, the induction was performed 1 d after surgery. All mice were closely monitored during tamoxifen injections and the post-injection period.

Immunohistochemistry. Immunohistochemistry experiments were performed following standard procedures. Briefly, mice were anesthetized with Euthasol (0.2 ml; Virbac) and transcardially perfused with 30 ml of PBS, followed by 30 ml of 4% paraformaldehyde (PFA) in PBS. Brains were extracted and further fixed in 4% PFA overnight followed by cryoprotection in a 30% PBS-buffered sucrose solution for 36 h at 4 °C. Coronal sections (50 µm in thickness) were cut using a freezing microtome (Leica SM 2010R). Brain sections were first washed in PBS (3 × 5 min), incubated in PBST (0.3% Triton X-100 in PBS) for 30 min at RT and then washed with PBS (3 × 5 min). Next, sections were blocked in 5% normal goat serum in PBST for 30 min at RT and then incubated with the primary antibody overnight at 4 °C. Sections were washed with PBS (5 × 15 min) and incubated with the fluorescent secondary antibody at RT for 2 h. After washing with PBS (5 × 15 min), sections were mounted onto slides with Fluoromount-G (eBioscience). Images were taken using an LSM 780 laser-scanning confocal microscope (Carl Zeiss).

The primary antibodies and dilutions used in this study were: rabbit anti-CaMKII (1:500; Abcam, ab52476, GR312537-6), rabbit anti-GABA (1:500; Sigma, A2052), chicken anti-GFP (1:1,000; Aves Labs, GFP1020, GFP697986), rabbit anti-RFP (1:1,000; Rockland, 600-401-379, 35868), rabbit anti-substance P (1:1,000; ImmunoStar, 20064, 1531001), rabbit anti-HA-tag (1:1,000; Cell Signaling, 3724S), rabbit anti-mCherry (1:1,000; Abcam, ab167453, GR3213077-3) and rabbit anti-DARPP32 (1:1,000; Abcam, ab40801). The fluorophore-conjugated secondary antibodies and dilutions used were Alexa Fluor 488 donkey anti-chicken IgG (H + L; 1:1,000; 703-545-155, Jackson ImmunoResearch), Alexa Fluor 488 goat anti-rabbit IgG (H + L; 1:1,000; A-11008, Invitrogen) and Alexa Fluor 555 goat anti-rabbit IgG (H + L; 1:1,000; A-21428; Life Technologies).

Fluorescence in situ hybridization. smFISH (RNAscope, ACDBio) was used to detect the expression of *Rspo2*, *Pppr1b1*, *Fezf2* and *Flp* mRNAs in the BLA of wild-type, *Fezf2-CreER* or *Fezf2-Flp* mice. We used the *Fezf2-CreER;H2B-GFP* mice, in which Fezf2^{BLa} neurons can be readily recognized by their expression of the nuclear GFP 3 weeks after tamoxifen induction. For tissue preparation, mice were first anesthetized under isoflurane and then decapitated. Their brain tissue was first embedded in cryomolds (Sakura Finetek, 4566) filled with M-1 Embedding Matrix (Thermo Scientific, 1310) then quickly fresh-frozen on dry ice. The tissue was stored at −80 °C until it was sectioned with a cryostat. Cryostat-cut sections (16-µm thick) containing the entire BLA were collected through the rostrocaudal axis in a series of four slides, and quickly stored at −80 °C until processed. Hybridization was carried out using the RNAscope kit (ACDBio).

On the day of the experiment, frozen sections were postfixed in 4% PFA in RNA-free PBS (hereafter referred to as PBS) at RT for 15 min, then washed in PBS, dehydrated using increasing concentrations of ethanol in water (50%, once; 70%, once; 100%, twice; 5 min each). Sections were then dried at RT and incubated with Protease IV for 30 min at RT. Sections were washed in PBS three times (5 min each) at RT, then hybridized. Probes against *Ppp1r1b* (405901-C3, dilution 1:50), *Rspo2* (402001-C1, dilution 1:50), *Fezf2* (888591-C2, dilution 1:50) and *Flp* (448191-C1, dilution 1:50) were applied to the BLA sections. Hybridization was carried out for 2 h at 40 °C. After that, sections were washed twice in 1× Wash Buffer (310091; 2 min each) at RT, then incubated with the amplification reagents for three consecutive rounds (30 min, 15 min and 30 min, at 40 °C). After each amplification step, sections were washed twice in 1× Wash Buffer (2 min each) at RT. Finally, fluorescence detection was carried out for 15 min at 40 °C. The green channel was kept available for the intrinsic nuclear GFP signals, which did not require amplification. Sections were then washed twice in 1× Wash Buffer (2 min each), incubated with DAPI for 2 min, washed twice in 1× Wash Buffer (2 min each), then mounted with a coverslip using mounting medium. Images were acquired using an LSM780 confocal microscope equipped with ×20 and ×40 lenses, and visualized and processed using ImageJ and Adobe Illustrator.

Behavioral tasks. *Th active approach and avoidance task.* Th s task was designed to train mice to actively seek reward and actively avoid punishment. Mice were subjected to water deprivation starting from 23 h before the training, during which they were head restrained using custom-made clamps and metal head bars. Each mouse was fi st habituated to the head restraint for 2–4 d, one session (1 h) per day. Unpredicted drops of water (5 µl) were delivered through a metal spout placed next

to the mouth of the mice during habituation. Once animals had learned how to obtain water by licking the spout, they were subjected to conditioning that included different types of trials. In the reward trials, a 1-s 4-kHz tone (CS_R) was presented, followed by a 2-s decision window. If mice licked the spout at least once during the decision window, water (5 µl) would be delivered through the spout immediately after this window. Otherwise, no water would be delivered. In the punishment trials, a 1-s 12-kHz tone (CS_P) was presented, followed by a 2-s decision window. If mice ran above a threshold speed (10 cm s^{-1}) during the decision window, they would avoid an unpleasant air puff (4 psi, 100 ms) blowing to the face, in an area close to the eye. Otherwise, mice would receive the air puff im ediately after the decision window.

For the behavioral training in GCaMP6 imaging or photometry experiments, we added neutral trials, in which a 1-s 8-kHz tone or white noise (CS_N) was presented. The CS_N was followed by nothing and served as a control. We recorded neuronal activities during both the early and the late training stages for all the mice used in these experiments. The early stage was the first training session. The late stage was defined as when the animals reached a threshold performance level (80%) in both the reward and the punishment trials.

Animals were trained during one session per day, with each session consisting of 200 trials if the neutral trials were not included, or 300 trials if the neutral trials were included. The different types of trials were randomly interleaved. The intertrial interval was randomly variable between 10 to 20 s. To reduce photobleaching, each imaging session consisted of 60 trials in total, with 20 trials being allocated for each of the three trial types.

Real-time place preference or aversion test. Freely moving mice were initially habituated to a two-sided chamber (23 × 33 × 25 cm for each chamber; made from Plexiglas) for 10 min, during which their baseline preference for the left or right side of the chamber was assessed. During the first test session (10 min), we assigned one side of the chamber (counterbalanced across mice) as the photostimulation side, and placed the mice in the non-stimulation side to start the experiment. Once the mouse entered the stimulation side, photostimulation (5-ms pulses, 30 Hz, 10 mW (measured at the tip of optic fibers)), generated by a 473-nm laser (OEM Laser Systems), was immediately turned on, and was turned off as soon as the mouse exited the stimulation side. In the second test session (10 min), we repeated this procedure but assigned the other side of the chamber as the stimulation side. The behavior of the mice was videotaped with a CCD camera (C930, Logitech) interfaced with Ethovision software (Noldus Information Technologies), which was also used to control the laser stimulation and extract behavioral parameters (position, time, distance and velocity). We used a preference score as a measure of the effect of laser stimulation, which was calculated as: $(\text{time in stimulation side} - \text{time in non-stimulation side})_{\text{stimulation}} - (\text{time in stimulation side} - \text{time in non-stimulation side})_{\text{baseline}}$, that is, the difference in time spent in the stimulation side and non-stimulation side during the stimulation session, subtracted by the difference in time spent in the two corresponding sides during the baseline session (to correct baseline bias). A positive score indicates preference for the stimulation side.

Intracranial self-stimulation test. Mice were tested in a chamber equipped with two ports. In each test session (1 h in duration), mice were allowed to freely explore and poke into both ports. Poking into one of the ports (the active port) would trigger a laser and thus lead to photostimulation in the OT for 2 s (5-ms pulses, 30 Hz, 10 mW; $\lambda = 473$ nm). Poking into the other port (the inactive port) would not trigger the photostimulation. Twenty-four hours later, the test was repeated, with a different port being designated as the active port. The poking events during each session were recorded and analyzed by a custom script written in MATLAB (The MathWorks).

In vivo chemogenetic inhibition. To test the behavioral effects of inhibiting $Fezf2^{BLa}$ neurons in the AAA task, we expressed KORD (a DREADD derived from the kappa-opioid receptor)[40] or GFP (as the control) into these neurons in mice with the respective viruses, and treated these mice with the KORD agonist SALB[40] (10 mg per kg of body weight, subcutaneous injection) 15 min before behavioral testing.

In vivo optogenetic inhibition and activation. For optogenetic inhibition in the BLa during learning in the AAA task, laser stimulation (4-s square pulse, $\lambda = 473$ nm, 10 mW measured at the tip of optical fiber) was delivered following the onset of CS presentation in each trial, to cover both CS and US presentation. For optogenetic inhibition after learning in this task, the laser pulse (3 s in duration) was delivered following the onset of CS presentation to cover CS presentation and decision window, in a randomly selected subset (~50%) of trials.

To determine whether activation of $Fezf2^{BLa \rightarrow NAc}$ neurons or their axon terminals could drive negative reinforcement learning, we used the same design as that for the punishment trials in the AAA task, but replaced the air puff with a 2-s train of optogenetic stimulation (5-ms pulses, 30 Hz, 10 mW; $\lambda = 473$ nm) of these neurons. Mice were trained during one session (100 trials) per day, with each trial beginning with a 1-s 2-kHz tone, followed by a 2-s decision window. The intertrial interval was randomly variable between 5 to 10 s.

Behavioral data collection and analysis. An open-source Bpod behavioral control system (Sanworks) was used to control real-time animal behavior and optogenetic manipulation. Custom-written scripts in MATLAB based on Bpod commands were used to control the delivery of CS and US and record behavioral responses, including licking events and running velocity. Pure tones (70 db; the CS) with different frequencies were generated as sine waves. The tones were uploaded to the audio adaptor board using the Bpod control system. The amount of water (the reward US) was controlled by fast solenoid valves (The Lee Company). A metal spout was placed in front of the mouth of an animal for water delivery. The spout also served as part of a custom 'lickometer' circuit, which registered a lick event each time a mouse completed the circuit by licking the spout. The licking events were recorded and analyzed using custom scripts written in MATLAB. Air-puff delivery (the aversive US) was controlled by a solenoid valve (U.S. Solid) with a higher-pressure operating limit. The air puff (40 psi) was delivered through a metal tube pointing toward the area surrounding the eye. We used a rotary encoder (YUMO-E6B2-CWZ3E-1024; SparkFun Electronics) to detect and record real-time running velocity. The rotary encoder was attached to a running wheel and connected with a microcontroller (Arduino UNO R3; SparkFun Electronics). The running wheel (diameter, 14 cm; width, 8 cm) was made using a three-dimensional printer (MakerBot Replicator 2; MakerBot). The microcontroller converted the digital inputs from the rotary encoder into analog signals reflecting running velocity, which was in turn recorded and analyzed with custom scripts written in MATLAB.

Pupil size measurement and analysis. To measure pupil size changes, we captured a video of an area surrounding the eye using an infrared-filter mounted camera (20 Hz, FL3-U3-13S2C-CS, Point Grey) under lighting with infrared light-emitted diodes. The camera was controlled by open-source Bonsai software. Offline video analysis was conducted using EthoVision XT software (Noldus). To measure pupil size, we manually selected a region of interest (ROI) surrounding the pupil. Pixels corresponding to the pupil were assigned as those that were darker than the surrounding background within the ROI. To quantify the changes in pupil size (ΔA), we computed $\Delta A/A_0(t) = (A(t) - A_0)/A_0$, where A_0 is the mean size of the area corresponding to the pupil during the baseline before laser stimulation and $A(t)$ is the pupil size in each picture frame, using a custom script written in MATLAB.

In vivo calcium imaging and data analysis. We performed calcium imaging using a custom-built wide-field one-photon fluorescence microscope equipped with an objective lens (×10, NA 0.3, MPlanFLN, Olympus) and an LED fluorescent light source (pE-100, CoolLED). The light was band-pass filtered (FF02-482/18-25, Semrock) to obtain the desired excitation wavelength, and reflected by a dichroic mirror (FF409/493/573/652-Di01, Semrock) to be collected by the objective through the back aperture, and was relayed by the implanted GRIN lens to reach neurons of interest. The emission fluorescence signals coming back through the same GRIN lens were collected by the objective and passed through an emission filter (FF01-520/35-25, Semrock) before they were recorded by a CCD camera (PCO. Pixelfly, PCO-Tech), which was controlled by software written in LabView (National Instruments).

All imaging experiments were conducted on awake behaving mice under head restraint in a dark, sound-attenuated box. We imaged neuronal activities before and throughout behavioral training. To reliably detect stimulus-driven responses while minimizing photobleaching, we typically imaged neuronal responses in the same condition in 20 trials, with the imaging duration for each trial being 20 s to cover baseline, CS and/or US responses. During the pre-learning habituation, we imaged the responses to either CS or US, which were presented randomly interleaved. During conditioning, we carefully adjusted the camera to image neurons in the same focal plane as that in the pre-learning sessions.

For imaging data processing and analysis, we first used Mosaic software (version 1.0.0b; Inscopix) to combine all the video frames from one imaging session into a single image stack (in TIFF format). The image stack was then spatially downsampled by a factor of 4. Motion artifacts were corrected using image registration techniques in the Mosaic environment to align all movie frames to a single target image and generate a stable, motion-corrected movie. Briefly, there were three steps in the motion-correction process: (1) generating the target image, (2) running the image registration routine, and (3) removing the post-registration border.

The first step in the motion-correction process was to generate a target image for the image registration routine. For this purpose, we chose a single frame from a movie and extracted the frame using the 'extract frame' app in Mosaic, which was subsequently used as the target image for correcting the motion artifacts in this movie. The target image was chosen carefully such that it was representative of the entire movie and did not exhibit any unusual fluorescence signals.

The second step in the motion-correction process was to set up and run the image registration algorithm using the 'apply motion correction' app in Mosaic. This step included adjusting the contrast of the target image and selecting a reference region that had high contrast pixels and vasculature areas. The image registration algorithm aligns each frame in the movie to the reference region in the target image and outputs a new, motion-corrected movie.

The third step was to remove the post-registration border. The movies generated in the second step usually contain sections of black pixels around the

edges of individual image frames. These black border areas are generated after the registration process as the image registration algorithm fills the pixels that fall outside the acquired frame with a null value. For more detailed information about the motion-correction process, see https://support.inscopix.com/sites/default/files/sphinx/1547/html/tutorials/standardWorkflow.html.

Next, we applied the extended constrained nonnegative matrix factorization (CNMF-E)[58–60], which is optimized for one-photon imaging, to demix neural signals and get their denoised and deconvolved temporal activity (Supplementary Video 1), termed ΔF[59,60]. The CNMF-E method was carried out using a custom MATLAB algorithm (see ref. [59] for a detailed description of this method). The contours of neurons in Fig. 2a and Supplementary Video 1 were generated by the CNMF algorithm on the basis of values eight standard deviations (s.d.) above the mean in a spatial component matrix, which are pixel-by-pixel-weighted fluorescence values.

To determine whether a neuron was significantly ($P<0.05$) excited or inhibited by a stimulus, and thus can be classified as being 'responsive' to the stimulus, we performed the Wilcoxon signed-rank test on the data acquired from 20 trials per stimulus, which compared the mean ΔF values in two 3-s time windows using all these trials, with one window immediately preceding stimulus onset and the other immediately following stimulus onset. To obtain the temporal z-scores for a neuron, we first obtained the mean activity trace for the neuron by averaging the fluorescence signals (ΔF) at each time point across all trials, and then computed the z-scores as $(F(t)-Fm)$/s.d., where $F(t)$ is the ΔF value at time t, Fm and s.d. are the mean and standard deviation, respectively, of the ΔF values over the baseline period. For the trial-by-trial analyses, the z-scores were computed for each trial using the same method (but without the averaging across trials).

Cell registration. To identify the same individual cells from images acquired from different imaging sessions, we performed cell registration using a probabilistic method that automatically registers cells across multiple imaging sessions and estimates the registration confidence for each registered cell[61]. Briefly, as we previously described[58], we first used CNMF-E analysis to generate the spatial footprints for all cells imaged in the pre-learning session. We then repeated this process for the cells imaged in the post-learning sessions. We used the footprints from the pre-learning session as a reference map, and aligned with this map the footprints from the post-learning sessions by correcting for translation and rotation differences between different sessions. We subsequently calculated the probability of a given pair of cells, each from one of two imaging sessions, to be the same cell (P_{same}) based on their spatial correlation and centroid distance. A pair of cells is considered to have the same identity if $P_{same}>0.5$. The centroid distance between a pair of cells deemed to have the same identity is generally small (≤6 μm).

Classification of neurons with clustering analysis. To classify neurons based on their CS response profiles after learning, we performed PCA on the z-scores representing the CS responses of these neurons, as previously described[58]. We subsequently applied hierarchical clustering analysis to the first three principal components using a correlation distance metric and complete agglomeration methods.

Decoding analysis. We used the SVM algorithm (fitcsvm) in MATLAB to examine whether different trial types could be predicted on the basis of populational CS responses of Fezf2^{BLa} neurons acquired in each mouse at different stages of learning. We used z-scores to represent the trial-by-trial responses of each neuron to presentations of CS_R, CS_N or CS_P during the early or late stage of learning. For each mouse, we captured the trial-by-trial population CS responses by a vector containing the responses of all neurons from that mouse, with each neuron representing one dimension in a multidimensional population space. We applied PCA on the multidimensional data from each mouse and used the first two principal components to represent the population response in each trial. We then used the low-dimensional trial-by-trial population responses from each mouse to train and test an SVM decoder with a Gaussian kernel to distinguish between reward, punishment and neutral trials. Specifically, we used the responses from 60 trials (20 CS_R, 20 CS_N and 20 CS_P) for each mouse during either the early or the late training stage to train and test a classifier. For decoder training and testing, we used a tenfold cross-validation procedure, in which all datasets were randomly partitioned to ten equal-sized subsamples, with each subsample containing an equal number of responses from a given class (that is, CS_R, CS_N or CS_P). We used nine of the ten subsamples for training and determining the boundary that optimally separated reward, neutral and punishment trials. The remaining one subsample was used for validating the decoder. We repeated this process ten times such that each of the ten subsamples was used exactly once as the validation data. The percentage of accurate classification incidence in the ten times was reported as the final classification accuracy.

In vivo fiber photometry and data analysis. To record the activities of Fezf2^{BLa} neurons projecting to the NAc or OT in vivo in behaving animals, we used a commercial fiber photometry system (Neurophotometrics) to measure GCaMP6 signals in these neurons through an optical fiber (fiber core diameter, 200 μm; fiber length, 5.0 mm; NA, 0.37; Inper) implanted in the BLa. A patch cord (fiber core diameter, 200 μm; Doric Lenses) was used to connect the photometry system with the implanted optical fiber. The intensity of the blue light ($\lambda=470$ nm) for excitation was adjusted to ~20 μW at the tip of the patch cord. Emitted GCaMP6f fluorescence was band-pass filtered and focused on the sensor of a CCD camera. Photometry signals and behavioral events were aligned based on an analog TTL signal generated by the Bpod. Mean values of signals from a ROI were calculated and saved by using Bonsai software, and were exported to MATLAB for further analysis.

To correct potential photobleaching of fluorescence signals, we subtracted the slow fluctuations in baseline according to $F\_raw\_correction(t)=F\_raw(t)-F\_norm(t)+F\_average$, where F_raw($t$) is the raw fluorescence at time t, F_norm(t) is the average of F_raw over a 100-s sliding window around time t, and F_average is the averaged fluorescence of F_raw over the entire recording time. The $\Delta F/F_0$ was calculated by $(F\_raw\_correction(t)-F_0)/F_0$, where F_0 is the averaged F_raw_correction during the baseline period.

In vitro electrophysiology. Patch-clamp recording was performed as previously described[62]. Briefly, mice were anesthetized with isoflurane (4%) before they were decapitated. The brains were then dissected out and placed in ice-chilled dissection buffer (110 mM choline chloride, 25 mM $NaHCO_3$, 1.25 mM NaH_2PO_4, 2.5 mM KCl, 0.5 mM $CaCl_2$, 7.0 mM $MgCl_2$, 25.0 mM glucose, 11.6 mM ascorbic acid and 3.1 mM pyruvic acid, gassed with 95% O_2 and 5% CO_2). An HM650 Vibrating-blade Microtome (Thermo Fisher Scientific) was then used to cut 300-μm-thick coronal sections that contained the NAc and OT. These slices were subsequently transferred to a storage chamber that contained oxygenated artificial cerebrospinal fluid (ACSF; 118 mM NaCl, 2.5 mM KCl, 26.2 mM $NaHCO_3$, 1 mM NaH_2PO_4, 20 mM glucose, 2 mM $MgCl_2$ and 2 mM $CaCl_2$, at 34 °C, pH 7.4, gassed with 95% O_2 and 5% CO_2). Following 40 min of recovery time, slices were transferred to RT (20–24 °C), where they were continuously bathed in the ACSF.

Whole-cell patch-clamp recording from NAc or OT neurons was obtained with Multiclamp 700B amplifiers and pCLAMP 10 software (Molecular Devices), and was visually guided using an Olympus BX51 microscope equipped with both transmitted and epifluorescence light sources (Olympus). The external solution was ACSF with tetrodotoxin (1 μM) and 4-aminopyridine (200 μM) added. The internal solution contained 115 mM cesium methanesulfonate, 20 mM CsCl, 10 mM HEPES, 2.5 mM $MgCl_2$, 4 mM Na_2ATP, 0.4 mM Na_3GTP, 10 mM sodium phosphocreatine and 0.6 mM EGTA (pH 7.2).

As the acute slices were prepared from mice in which Fezf2^{BLa} neurons were infected with an AAV expressing ChR2-YFP, to evoke synaptic transmission onto either NAc or OT neurons driven by Fezf2^{BLa} neurons, a blue light was used to stimulate ChR2-expressing axons originating from Fezf2^{BLa} neurons. The light source was a single-wavelength LED system ($\lambda=470$ nm; https://www.coolled.com/) connected to the epifluorescence port of the Olympus BX51 microscope. A light pulse of 1 ms, triggered by a TTL signal from the Clampex software, was delivered every 10 s to drive synaptic responses. Synaptic responses were recorded at a holding potential of −85 mV, low-pass filtered at 1 kHz and were analyzed using pCLAMP 10 software. Comparable number of neurons were recorded from the NAc or OT from each slice.

Mapping monosynaptic inputs with pseudotyped rabies virus. To map the brain-wide monosynaptic inputs onto Fezf2$^{BLa\rightarrow NAc}$ and Fezf2$^{BLa\rightarrow OT}$ neurons, we used a pathway-specific and cell-specific tracing strategy[35] with an optimized rabies virus system[36]. We injected the NAc or OT of *Fezf2-CreER* mice with the retrograde CAV-Flex-FlpO, which allows the FlpO to be specifically expressed in Fezf2$^{BLa\rightarrow NAc}$ or Fezf2$^{BLa\rightarrow OT}$ neurons, respectively, flowing tamoxifen induction. A small amount of blue fluorescent beads was added to the CAV-Flex-FlpO viral solution to mark the injection site for histologic verification. Subsequently, in the same surgery, we injected the BLa of these mice with AAV-fDIO-TVA-mCherry and AAV-fDIO-oG (1:1 in volume, for a total of 0.3–0.4 μl) that express the following components in a Flp-dependent manner: a fluorescent reporter mCherry, TVA (which is a receptor for the avian virus envelope protein EnvA), and the rabies envelope glycoprotein (oG). Tamoxifen induction was performed in these mice 1 d after the surgery. Three weeks after the first injection, mice were injected in the BLa with Rbv-CVS-N2c-dG-GFP (0.5 μl), a rabies virus that is pseudotyped with EnvA, lacks the envelope glycoprotein, and expresses GFP. This rabies strain has been shown to have enhanced retrograde trans-synaptic transfer and reduced neurotoxicity[36]. Brain tissue was prepared 1 week after the rabies virus injection for histologic examination. This method ensures that the rabies virus exclusively infects the cells that express TVA, that is, the Fezf2$^{BLa\rightarrow NAc}$ or Fezf2$^{BLa\rightarrow OT}$ neurons. Furthermore, complementation of the modified rabies virus with the envelope glycoprotein in the TVA-expressing cells allows the generation of infectious particles, which can then infect presynaptic neurons via trans-synaptic release.

We followed a commonly used method to analyze the rabies tracing data[34,35,38,39,63–65]. Briefly, 50-μm coronal sections were obtained across the anteroposterior axis of the brain. We counted the number of GFP-labeled (that is, rabies-labeled) input cells in each brain structure throughout the entire brain, using every third brain section for the counting. Brain regions were identified on the basis of anatomical landmarks and defined according to Allen Brain Atlas. Data are presented as the ratio between the number of GFP-labeled cells in a given brain area and the total number of GFP-labeled cells in the entire brain.

Statistics and data presentation. All statistics are indicated where used. Statistical analyses were performed with MATLAB (MathWorks) or Prism software (GraphPad). We tested the normality of all data with the Kolmogorov–Smirnov normality test in MATLAB, and used nonparametric statistical tests for nonnormally distributed datasets, as indicated where used. All statistical tests were two sided and adjustments were made for multiple comparisons. Data collection and analysis were not performed blind to the conditions of the experiments. All behavioral experiments were controlled by computer systems, and data were collected and analyzed in an automated and unbiased way. No statistical methods were used to predetermine sample sizes, but our sample sizes are similar to those reported in previous publications[34,38,58]. An animal was excluded if the viral injection location (as indicated by a virally expressed fluorescent protein or co-injected blue beads) was outside the target area, such as the BLa, NAc or OT. If the tip of an implanted GRIN lens or optical fiber was outside the target area, or if the behavioral performance could not reach the threshold in the imaging and fiber photometry experiments, the mouse was also excluded. No other mice or data points were excluded.

Reporting Summary. Further information on research design is available in the Nature Research Reporting Summary linked to this article.

Data availability

All data are contained in the main text, extended data or Supplementary Information. Source data can be downloaded at https://figshare.com/articles/dataset/NN-A72265C/15130017.

Code availability

Source code can be downloaded at https://figshare.com/articles/software/code_for_NN-A72265C/15157614.

References

55. Taniguchi, H. et al. A resource of Cre driver lines for genetic targeting of GABAergic neurons in cerebral cortex. *Neuron* **71**, 995–1013 (2011).
56. He, M. et al. Strategies and tools for combinatorial targeting of GABAergic neurons in mouse cerebral cortex. *Neuron* **91**, 1228–1243 (2016).
57. Yu, K. et al. The central amygdala controls learning in the lateral amygdala. *Nat. Neurosci.* **20**, 1680–1685 (2017).
58. Zhang, X. & Li, B. Population coding of valence in the basolateral amygdala. *Nat. Commun.* **9**, 5195 (2018).
59. Zhou, P. et al. Effici t and accurate extraction of in vivo calcium signals from microendoscopic video data. *Elife* **7**, e28728 (2018).
60. Pnevmatikakis, E. A. et al. Simultaneous denoising, deconvolution, and demixing of calcium imaging data. *Neuron* **89**, 285–299 (2016).
61. Sheintuch, L. et al. Tracking the same neurons across multiple days in Ca^{2+} imaging data. *Cell Rep.* **21**, 1102–1115 (2017).
62. Li, H. et al. Experience-dependent modifi ation of a central amygdala fear circuit. *Nat. Neurosci.* **16**, 332–339 (2013).
63. Watabe-Uchida, M., Zhu, L., Ogawa, S. K., Vamanrao, A. & Uchida, N. Whole-brain mapping of direct inputs to midbrain dopamine neurons. *Neuron* **74**, 858–873 (2012).
64. Lerner, T. N. et al. Intact-brain analyses reveal distinct information carried by SNc dopamine subcircuits. *Cell* **162**, 635–647 (2015).
65. Beier, K. T. et al. Circuit architecture of VTA dopamine neurons revealed by systematic input–output mapping. *Cell* **162**, 622–634 (2015).

Acknowledgements

We thank T. Russo and R. Sharma for technical assistance, and members of the laboratory of B.L. for helpful discussions. This work was supported by grants from NARSAD (28229, to X.Z.; 27820, to K.Y.), EMBO (ALTF 458-2017, to A.F.), the Swedish Research Council (2017-00333, to A.F.), the NIH (R01MH101214, R01MH108924, R01NS104944 and R01DA050374, to B.L.; R01MH101268, to Z.J.H.), the Human Frontier Science Program (RGP0015/2016, to B.L.), the Stanley Family Foundation (to B.L.), the Simons Foundation (344904, to B.L.), the Wodecroft Foundation (to B.L.), the CSHL and Northwell Health Affiliation (to B.L.), Feil Family Neuroscience Endowment (to B.L.) and the Shanghai Rising-Star Program (18QA1400600, to M.H.).

Author contributions

X.Z. and B.L. conceived and designed the study. X.Z. conducted the experiments and analyzed data. W. Guan performed the patch-clamp recording experiments and assisted with rabies tracing experiments. T.Y. developed the one-photon wide-field imaging system and methods. A.F. performed the smFISH experiments. X.X. assisted with generating MATLAB codes for controlling behavioral devices. K.Y. assisted with the behavioral setup. X.A. and W. Galbavy assisted with characterization of *Fezf2*-expressing neurons. C.R and K.D. developed the Flp-off GCaMP6f virus. K.R. and A.H. developed the optimized rabies viral tracing system. M.H. designed and generated the *Fezf2-CreER* mouse line and characterized the labeling of neurons in the BLA. Z.J.H. conceived and oversaw the generation and characterization of the *Fezf2-CreER* and *Fezf2-Flp* mouse lines, and provided critical reagents and advice. X.Z. and B.L. wrote the paper with input from all authors.

Competing interests

The authors declare no competing interests.

Additional information

Extended data is available for this paper at https://doi.org/10.1038/s41593-021-00927-0.

Supplementary information The online version contains supplementary material available at https://doi.org/10.1038/s41593-021-00927-0.

Correspondence and requests for materials should be addressed to Xian Zhang or Bo Li.

Peer review information *Nature Neuroscience* thanks Anna Beyeler, Sabine Krabbe, and the other, anonymous, reviewer(s) for their contribution to the peer review of this work.

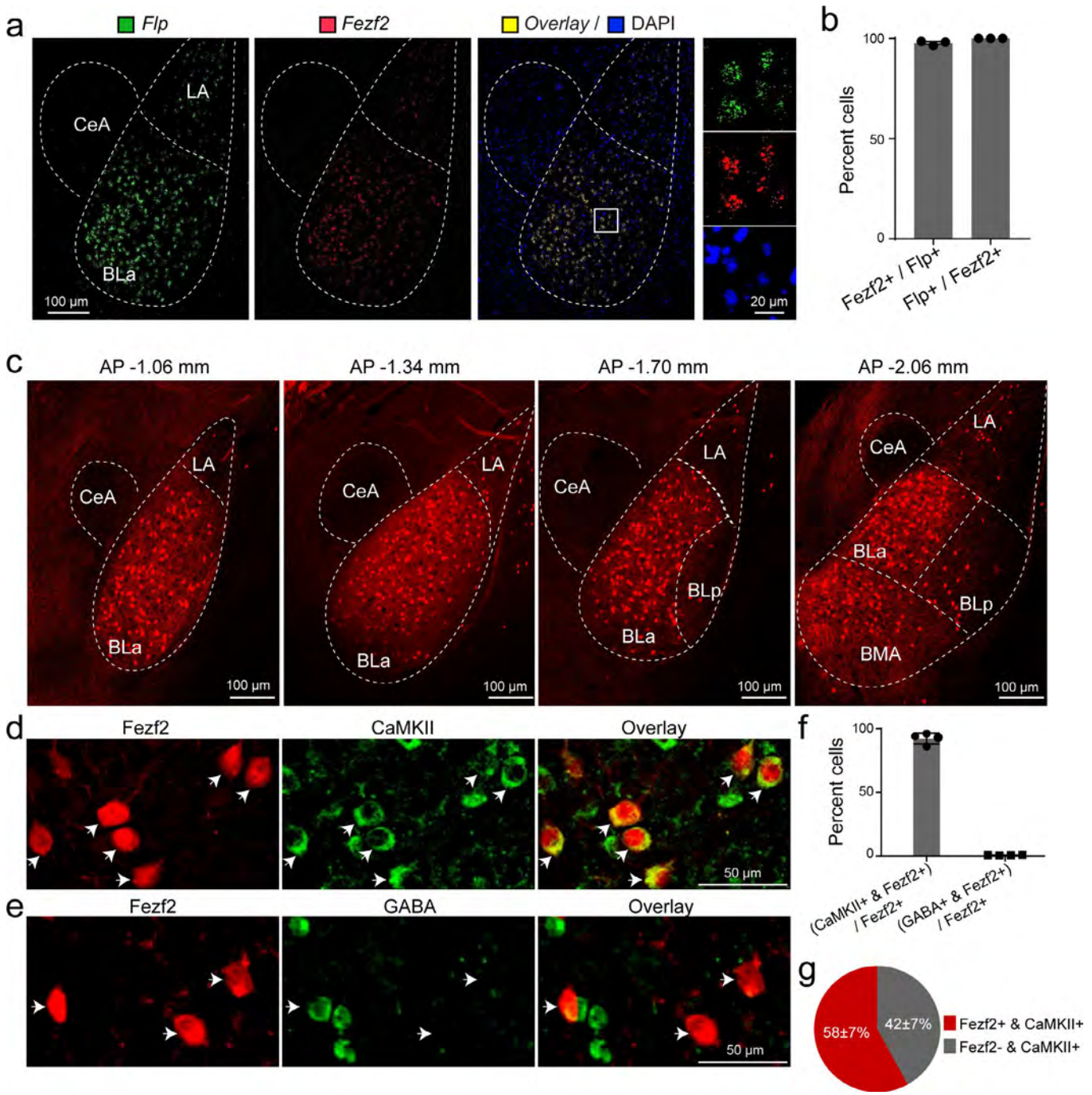

Extended Data Fig. 1 | Fezf2^{BLa} neurons constitute a subset of pyramidal neurons in the BLa. a, Confocal images of a coronal brain section containing the BLA from a *Fezf2-Flp* mouse, showing the distribution of *Flp* and *Fezf2* detected by smFISH, and overlay as indicated. In the right-most panel are high magnification images of the boxed area in the overlay image. **b**, Quantification of the fraction of *Flp*$^+$ neurons that co-express *Fezf2*, and vice versa (n = 3 mice). **c**, Confocal images of coronal brain sections from *Fezf2-CreER;Ai14* mice, in which *Fezf2*$^+$ neurons in the BLA are labeled with tdTomato (red). The BLa has the highest density of *Fezf2*$^+$ neurons within the BLA complex. This experiment was repeated in 4 mice. **d**, Representative confocal images showing Fezf2^{BLa} neurons labeled with tdTomato (left), BLa pyramidal neurons labeled by antibodies recognizing CaMKII (middle), and overlay (right). Arrows indicate Fezf2^{BLa} cells expressing CaMKII. **e**, Representative images showing Fezf2^{BLa} cells labeled with tdTomato (left), BLa inhibitory neurons labeled by antibodies recognizing GABA (middle), and overlay (right). Arrows indicate Fezf2^{BLa} cells that do not express GABA. **f**, Quantification of the fraction of Fezf2^{BLa} neurons that are pyramidal neurons or GABAergic neurons (n = 4 mice). **g**, Quantification of the fraction of BLa pyramidal neurons that are Fezf2$^+$ neurons or not (n = 4 mice). Data are presented as mean ± s.e.m.

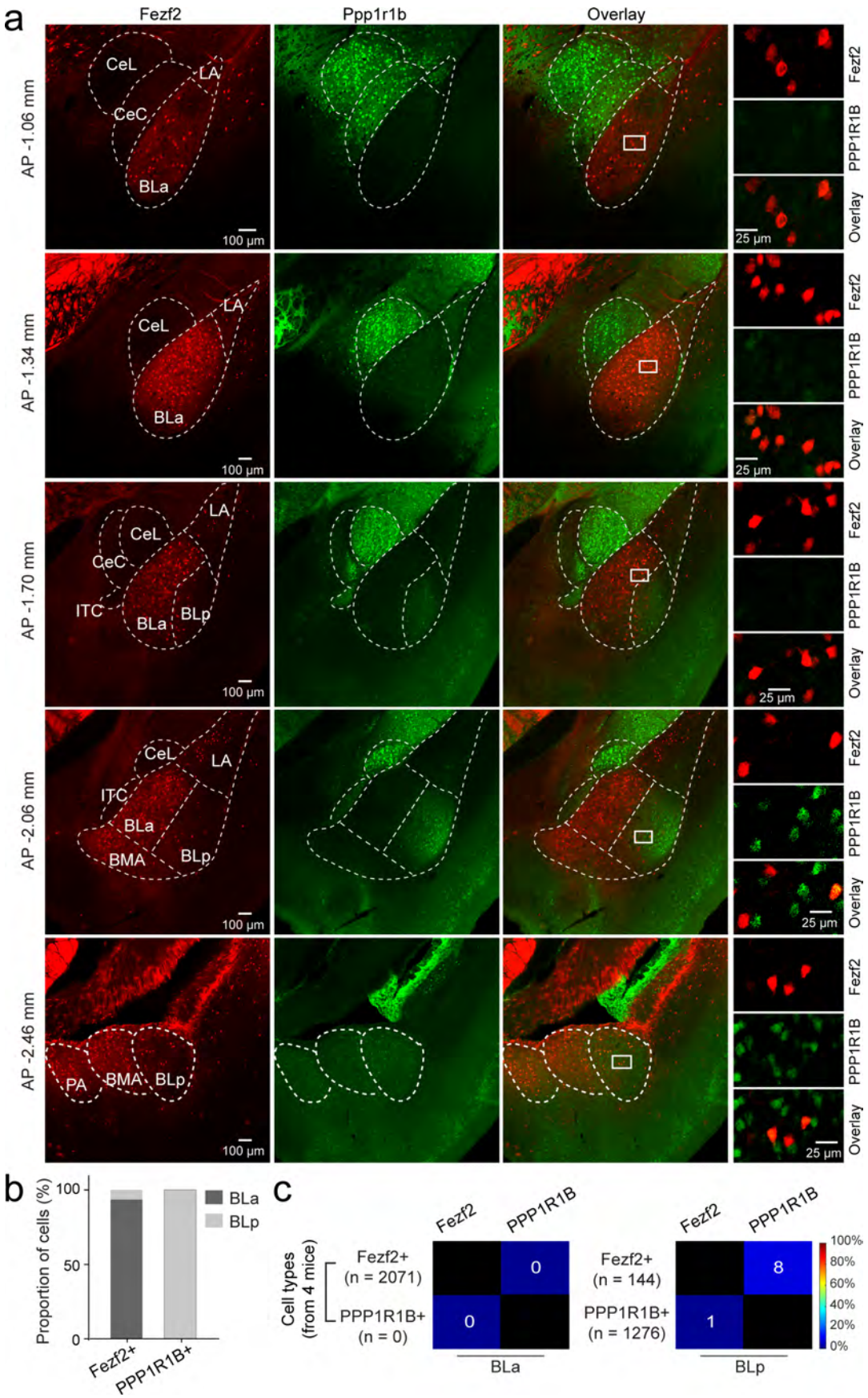

Extended Data Fig. 2 | See next page for caption.

Extended Data Fig. 2 | Fezf2^{BLa} neurons are not PPP1R1B^{+}neurons. a, Confocal images of coronal brain sections containing the BLA along the antero-posterior axis from a representative *Fezf2-CreER;Ai14 mouse, showing the distribution of Fezf2*$^{+}$ neurons labeled with tdTomato, and the distribution of PPP1R1B expression detected with antibodies. In the rightmost panel are high magnification images of the boxed area in the corresponding overlay images. **b**, Quantification of the distribution of Fezf2^{+} neurons and PPP1R1B^{+}neurons in the BLa and BLp (data from 4 mice). Note that the vast majority of Fezf2^{+} neurons are in the BLa, whereas essentially no PPP1R1B^{+}neurons are in the BLa. **c**, Quantification of the overlap between neurons that express Fezf2 and PPP1R1B in the BLa (left) and BLp (right) in the same mice as in (b). Values in matrix represent the percent labeling with markers in columns among neurons labeled with markers in rows. For example, in the BLa (left), 0% of Fezf2 (tdTomato)-labeled neurons were labeled with PPP1R1B.

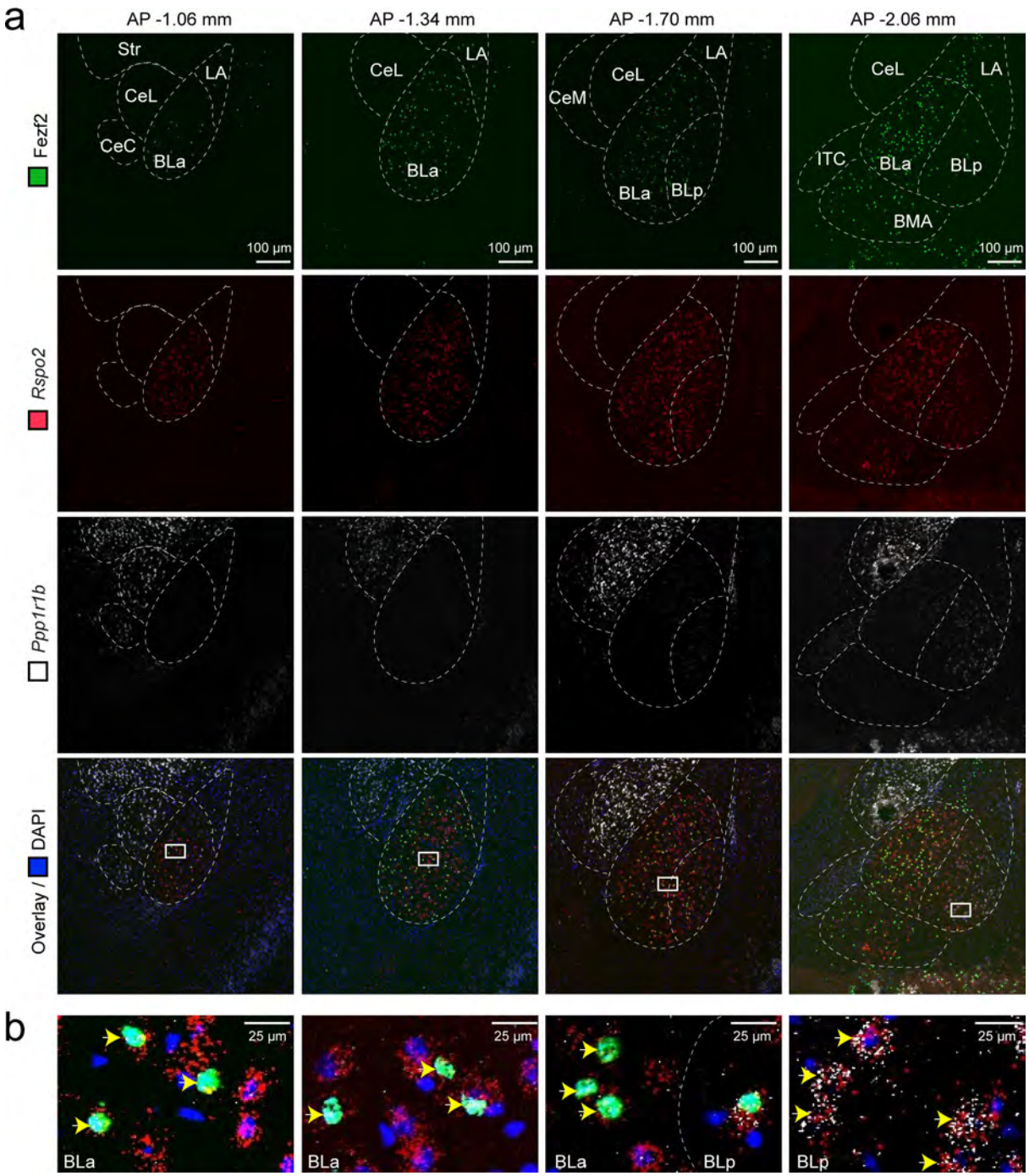

Extended Data Fig. 3 | Fezf2^{BLa} neurons are predominately *Rspo2*$^{+}$ neurons. a, Confocal images of coronal brain sections containing the BLA along the antero-posterior axis from a representative *Fezf2-CreER;H2B-GFP* mouse, showing the distribution of *Fezf2*$^{+}$ neurons labeled with H2B-GFP, and the distribution of *Rspo2* and *Ppp1r1b* expression detected with smFISH. This experiment was repeated in 2 mice. **b**, High magnification images of the boxed areas in the corresponding overlay images in (a). Arrows in the left three panels indicate that, in the BLa, *Fezf2*$^{+}$ neurons expressing *Rspo2*. Arrows in the rightmost panel indicate that, in the BLp, many *Ppp1r1b*$^{+}$ neurons express *Rspo2*, but not *Fezf2*. This experiment was repeated in 2 mice.

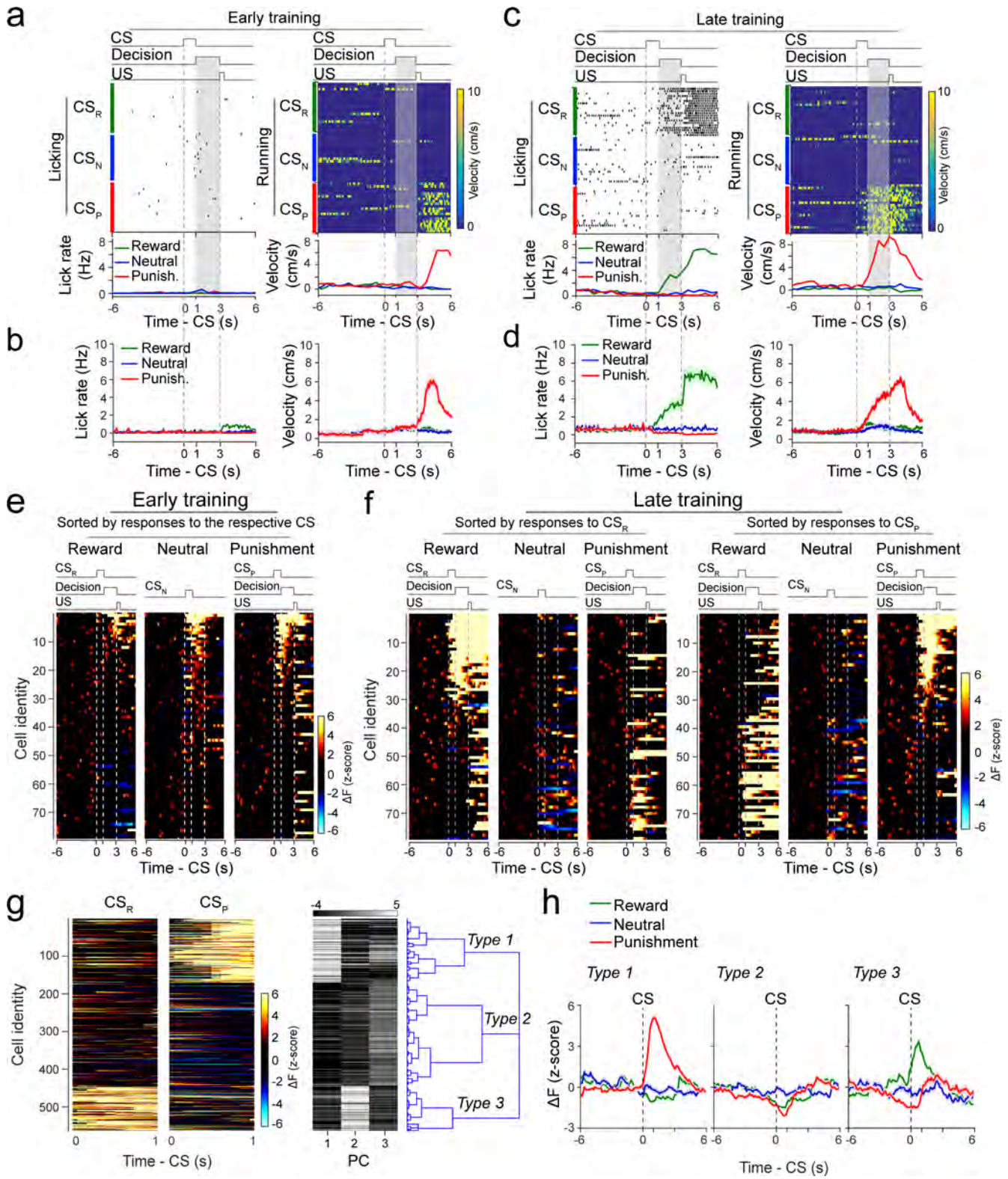

Extended Data Fig. 4 | See next page for caption.

Extended Data Fig. 4 | Characterization of behavior and Fezf2^{BLa} neuron activity in the AAA task. a, Top: licking (left) and running (right) events, sorted according to trial types, for a representative mouse in the early stage of training in the AAA task. Bottom: average licking rate (left) or running velocity (right) of this mouse in different types of trials as indicated. **b**, Average lick rate (left) and running velocity (right) of all the mice in the different types of trials in the AAA task during early stage of training. **c, d**, Same as (a, b), respectively, except that mice were in the late stage of training in the AAA task. **e**, Heatmaps of the activities (z-scores) in individual Fezf2^{BLa} neurons from a representative mouse, obtained from different types of trials in the early stage of training in the AAA task. Dashed lines indicate the onset of CS, decision window and US, as indicated. Each row in each type of trials (reward, neutral and punishment) represents the temporal activities of one neuron. Neurons are sorted according to their average z-scores during the presentation of different CSs. **f**, Left: heatmaps of the activities (z-scores) in individual Fezf2^{BLa} neurons from a representative mouse, obtained from different types of trials in the late stage of training in the AAA task. Dashed lines indicate the onset of CS, decision window and US as indicated. Each row represents the temporal activities of the same neuron in reward (left), neutral (middle) and punishment (right) trials. Neurons are sorted according to their average z-scores during the presentation of CS_R in the reward trials. Right: same dataset as that in the left, except that neurons are sorted according to their average z-scores during the presentation of CS_P in the punishment trials. **g**, Left: heat-maps of the responses of Fezf2^{BLa} neurons to CS_R (left) and CS_P (right) in the late training stage in the AAA task. Responses from all Fezf2^{BLa} neurons in all the mice (n = 10) are shown. Each row represents the responses of the same neuron to CS_R and CS_P. Right: PCA was applied to the CS responses in the left, followed by hierarchical clustering using the first three principal components (PCs) to sort Fezf2^{BLa} neurons into three clusters. **h**, The average responses of all neurons in each of the three clusters to different CSs. Data are presented as mean ± s.e.m. Shaded areas represent s.e.m.

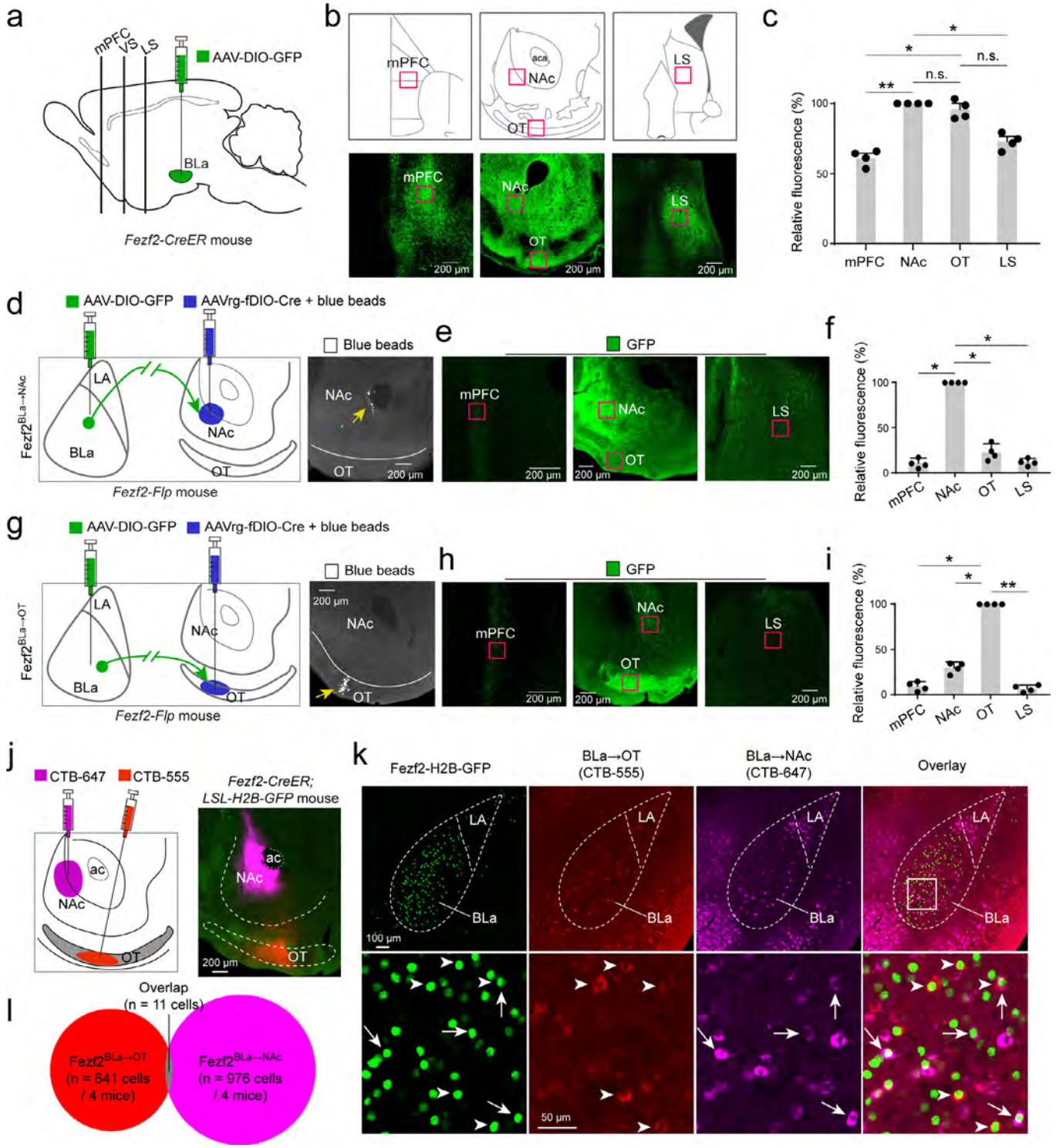

Extended Data Fig. 5 | See next page for caption.

Extended Data Fig. 5 | Anterograde and retrograde tracing of Fezf2^{BLa} neurons. a-i, Characterization of axonal projections from Fezf2^{BLa} neurons in target areas. **a**, A schematic of the approach and the sections used to quantify GFP fluorescence in the major target areas (mPFC, medial prefrontal cortex; VS, ventral striatum; LS, lateral septum). **b**, Upper: diagrams of the four major target areas. Lower: representative confocal images of coronal brain sections containing the corresponding target areas. Areas selected for analysis are marked by red boxes. **c**, Quantification of axonal fluorescence signals as the fluorescence intensity in target areas normalized by the intensity in the NAc for each animal (n = 4 mice; Friedman test (F-stat 11.1) with Dunn's post-hoc test: $P = 0.0009$; n.s., $P > 0.05$; $^{*}P < 0.05$; $^{**}P < 0.01$). **d**, Left: a schematic of the approach to selectively label Fezf2$^{BLa \rightarrow NAc}$ neurons. Right: a confocal image showing injection location of AAVrg-fDIO-Cre in the NAc, as indicated by fluorescent beads (arrow). **e**, Representative confocal images showing axons of Fezf2$^{BLa \rightarrow NAc}$ neurons in the mPFC (left), VS (middle) and LS (right). **f**, Quantification of Fezf2$^{BLa \rightarrow NAc}$ neuron axonal fluorescence signals. Data are represented as the fluorescence intensity in target areas normalized by the intensity in the NAc for each animal (n = 4 mice; Friedman test (F-stat 11.15) with Dunn's post-hoc test: $P = 0.0006$; n.s., $P > 0.05$; $^{*}P < 0.05$). **g**, Left: a schematic of the approach to selectively label Fezf2$^{BLa \rightarrow OT}$ neurons. Right: a confocal image showing injection location of AAVrg-fDIO-Cre in the OT, as indicated by fluorescent beads (arrow). **h**, Representative confocal images showing axons of Fezf2$^{BLa \rightarrow OT}$ neurons in the mPFC (left), VS (middle) and LS (right). **i**, Quantification of Fezf2$^{BLa \rightarrow OT}$ neuron axonal fluorescence signals. Data are represented as the fluorescence intensity in target areas normalized by the intensity in the OT for each animal (n = 4 mice; Friedman test (F-stat 11.1) with Dunn's post-hoc test: $P = 0.0009$; n.s., $P > 0.05$; $^{*}P < 0.05$; $^{**}P < 0.01$). **j-l**, Retrograde tracing of Fezf2$^{BLa \rightarrow NAc}$ and Fezf2$^{BLa \rightarrow OT}$ neurons with CTB. **j**, A schematic of the approach (left) and a histology image (right) showing CTB-647 and CTB-555 injected into the NAc and OT of *Fezf2-CreER;LSL-H2B-GFP* mice, respectively. **k**, Representative confocal images of the BLa in the same mouse as that in (j), showing Fezf2^{BLa} neurons labelled by H2B-GFP, CTB-555 and CTB-647. In the lower panel are high magnification images of the boxed area in the image in the upper panel. Arrowheads and arrows indicate the Fezf2$^{BLa \rightarrow OT}$ and Fezf2$^{BLa \rightarrow NAc}$ neurons, respectively; on the upper right corner (indicated by a vertical arrow) is a Fezf2^{BLa} neuron projecting to both the NAc and the OT (triple positive for H2B-GFP, CTB-555 and CTB-647). **l**, Quantification of the overlap between Fezf2$^{BLa \rightarrow OT}$ and Fezf2$^{BLa \rightarrow NAc}$ neurons. Data are presented as mean ± s.e.m.

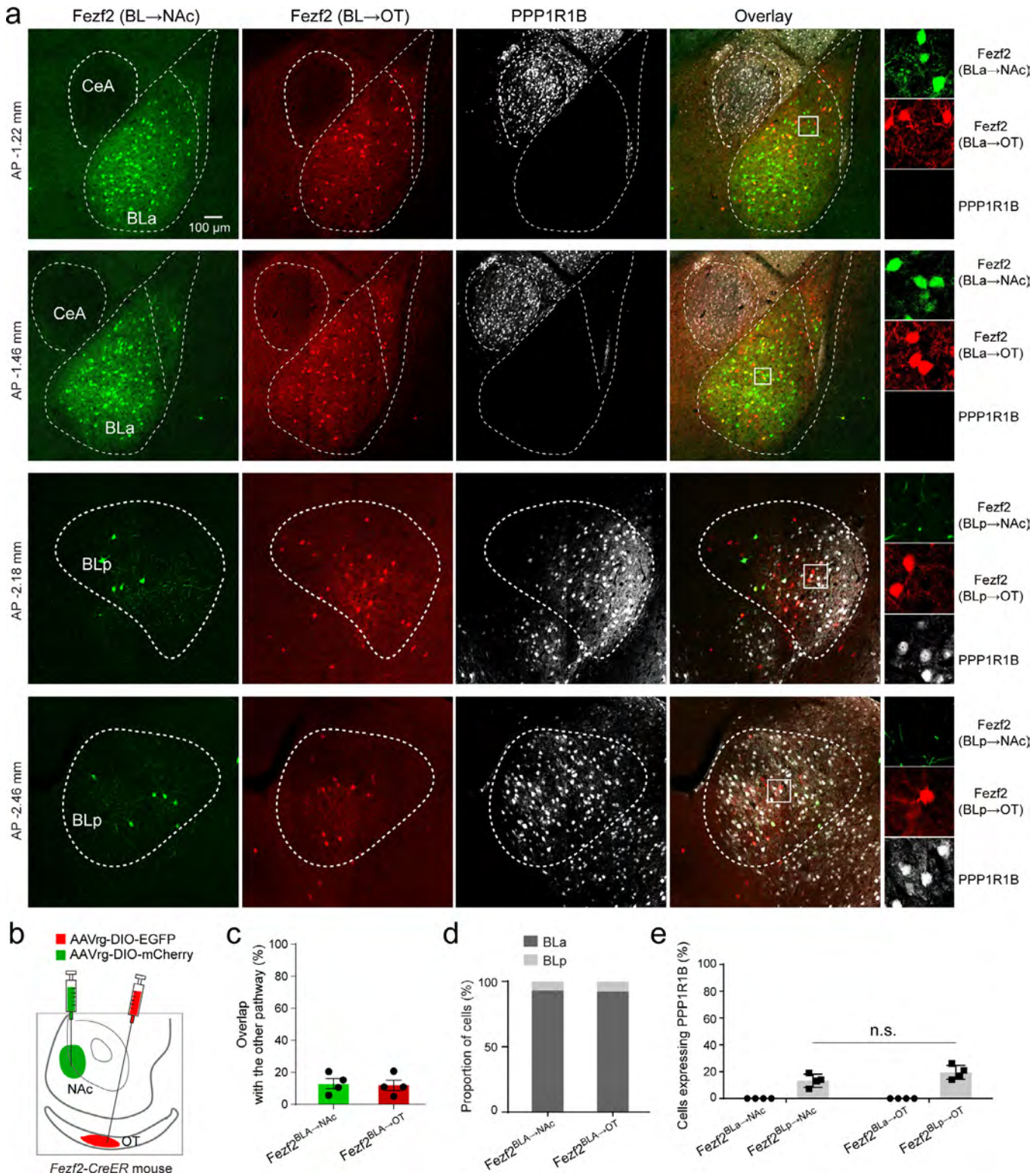

Extended Data Fig. 6 | Characterization of Fezf2$^{BLa\rightarrow OT}$ and Fezf2$^{BLa\rightarrow NAc}$ neurons. a, Confocal images of coronal brain sections containing the BLa or BLp along the antero-posterior axis from a representative *Fezf2-CreER mouse, showing the distribution of* NAc- or OT-projecting Fezf2^{+} neurons. In the rightmost panel are high magnification images of the boxed area in the corresponding overlay images. **b**, A schematic of the approach to target OT- or NAc-projecting Fezf2^{+} neurons in the BLA. **c**, Quantification of the proportion of overlapping neurons among Fezf2$^{BLA\rightarrow NAc}$ neurons (13 ± 3.1%) or Fezf2$^{BLA\rightarrow OT}$ neurons (11.8 ± 3.2%; 4 mice). **d**, Quantification of the OT- or NAc-projecting Fezf2^{+} neurons in the BLa and BLp. **e**, Quantification of the expression of PPP1R1B in NAc- or OT-projecting Fezf2^{+} neurons, in the BLa and BLp (n = 4; Friedman test (F-stat 10.1) with Dunn's post-hoc test: $P = 0.003$; n.s., $P > 0.05$). Data are presented as mean ± s.e.m.

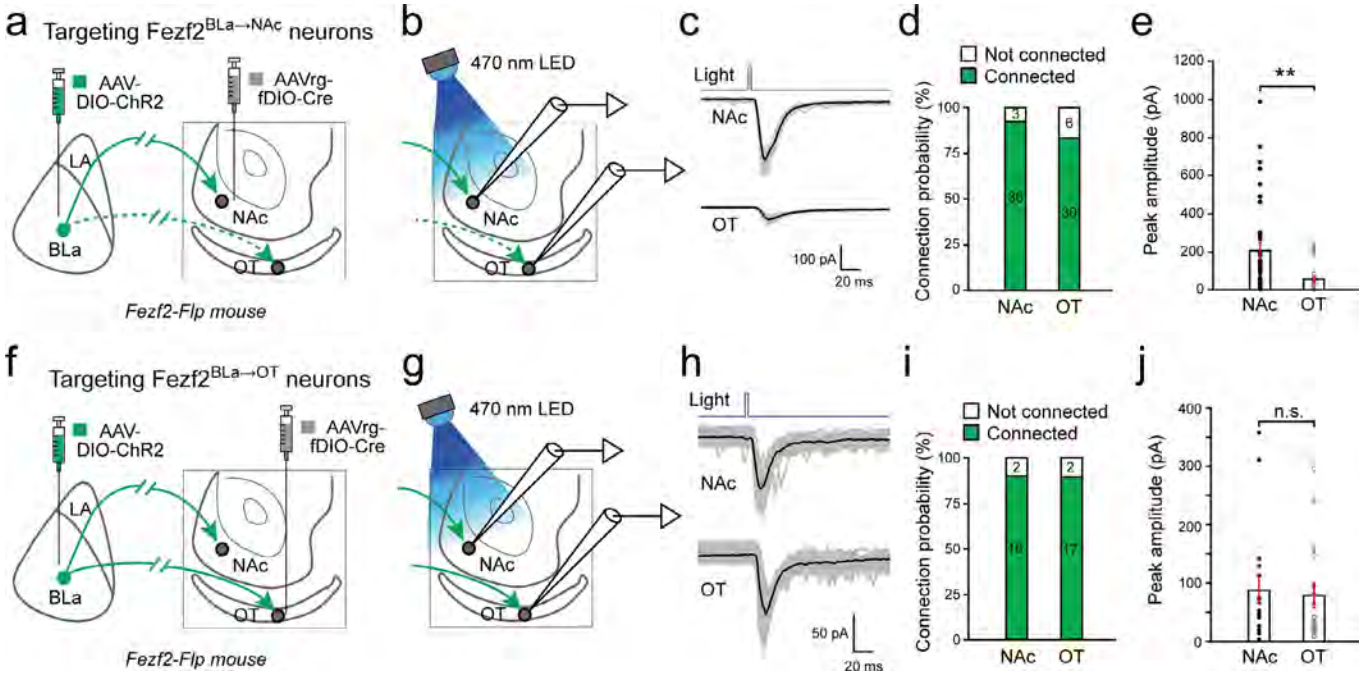

Extended Data Fig. 7 | Functional connectivity between Fezf2^{BLa} neurons and ventral striatum neurons. a, A schematic of the intersectional approach to selectively target Fezf2$^{BLa\rightarrow NAc}$ neurons for optogenetic activation. **b**, A schematic of the approach to record the synaptic responses of NAc and OT neurons to optogenetic activation of the axons originating from Fezf2$^{BLa\rightarrow NAc}$ neurons. **c**, Traces of excitatory postsynaptic currents (EPSCs) recorded from two representative neurons, with one in the NAc (top) and the other in the OT (bottom), in the presence of TTX and 4-AP. The EPSCs were evoked by optogenetic activation of axon fibers originating from Fezf2$^{BLa\rightarrow NAc}$ neurons. The upward square pulses (1 ms duration) in the blue traces (top) indicate the timing of photo-stimulation. **d**. Quantification of connection probability between Fezf2$^{BLa\rightarrow NAc}$ neurons and neurons in the NAc or OT (36 out of 39 cells in the NAc, and 30 out of 36 cells in the OT had evoked EPSCs). **e**, Quantification of peak amplitudes of the EPSCs (NAc, 36 cells, OT, 30 cells; 6 mice; **P = 0.0018, unpaired t test). **f-h**, Same as a-c, respectively, except that Fezf2$^{BLa\rightarrow OT}$ neurons were selectively targeted for optogenetic activation. **i**. Quantification of connection probability between Fezf2$^{BLa\rightarrow OT}$ neurons and neurons in the NAc or OT (18 out of 20 cells in the NAc, and 17 out of 19 cells in the OT had evoked EPSCs). **j**, Quantification of peak amplitudes of the EPSCs (NAc, 18 cells, OT, 17 cells; 4 mice; n.s., P = 0.78, unpaired t test). Data are presented as mean ± s.e.m.

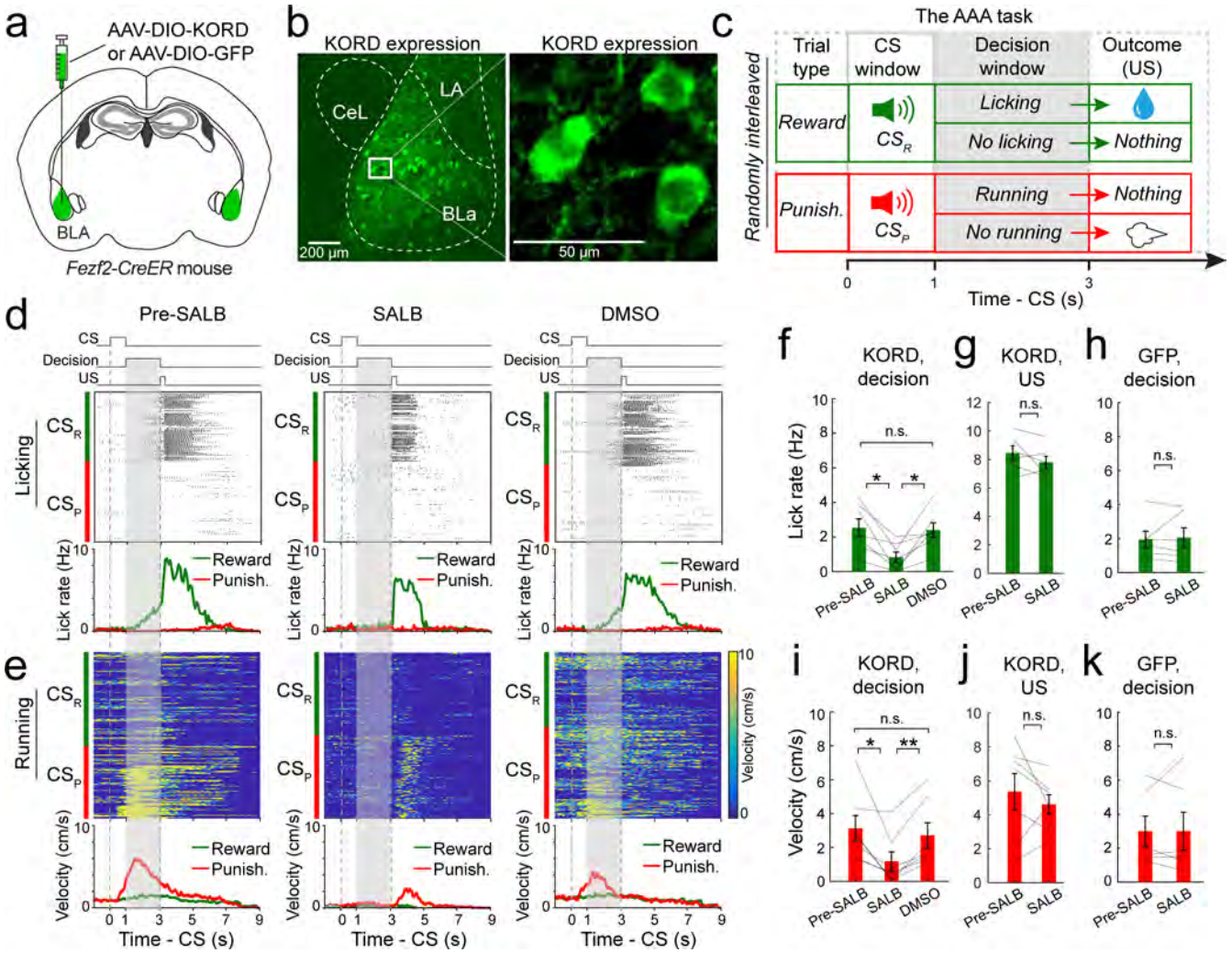

Extended Data Fig. 8 | Chemogenetic inhibition of Fezf2^{BLa} neurons impairs both reward seeking and punishment avoidance. a, A schematic of the approach. **b**, Representative confocal images showing the BLa neurons expressing KORD. **c**, A schematic of the AAA task. **d**, Top: licking events sorted according to trial types (which were randomly interleaved) for a representative mouse before (left), during (middle) and after (right) chemogenetic inhibition of Fezf2^{BLa} neurons. Bottom: the average rate of the licking responses in the corresponding top panels. **e**, Top: running events sorted according to trial types (which were randomly interleaved) for a representative mouse before (left), during (middle) and after (right) chemogenetic inhibition of Fezf2^{BLa} neurons. Bottom: the average velocity of the running responses in the corresponding top panels. **f**, Chemogenetic inhibition of Fezf2^{BLa} neurons reduced the licking responses during the decision window (n = 7 mice; $F(2, 18) = 5.13$, $P = 0.01$; Pre-SALB and SALB, $^*P = 0.0211$; SALB and DMSO, $^*P = 0.0299$; Pre-SALB and DMSO, n.s. (nonsignificant), $P = 0.97$; one-way ANOVA followed by Tukey's multiple comparisons test). **g**, Chemogenetic inhibition of Fezf2^{BLa} neurons did not affect the licking responses evoked by water (US) delivery to the mouth (n = 7; $t(6) = 1.4$, $P = 0.22$; paired t-test). **h**, Treatment with SALB does not change the licking responses during the decision window in control mice in which the Fezf2^{BLa} neurons expressed GFP (n = 6; $t(5) = -0.33$, $P = 0.75$; paired t-test). **i**, Chemogenetic inhibition of Fezf2^{BLa} neurons reduced the running responses during the decision window (n = 7 mice; $F(2, 18) = 3.95$, $P = 0.03$; Pre-SALB and SALB, $^*P = 0.0386$; SALB and DMSO, $^*P = 0.0048$; Pre-SALB and DMSO, n.s. (nonsignificant), $P = 0.6742$; one-way ANOVA followed by Tukey's multiple comparisons test). **j**, Chemogenetic inhibition of Fezf2^{BLa} neurons did not affect the running responses evoked by air-puff (US) blowing to the face (n = 7; $t(6) = 0.95$, $P = 0.38$; paired t-test). **k**, Treatment with SALB does not change the running responses during the decision window in control mice in which the Fezf2^{BLa} neurons expressed GFP (n = 6; $t(5) = -0.02$, $P = 0.98$; paired t-test). Data are presented as mean ± s.e.m.

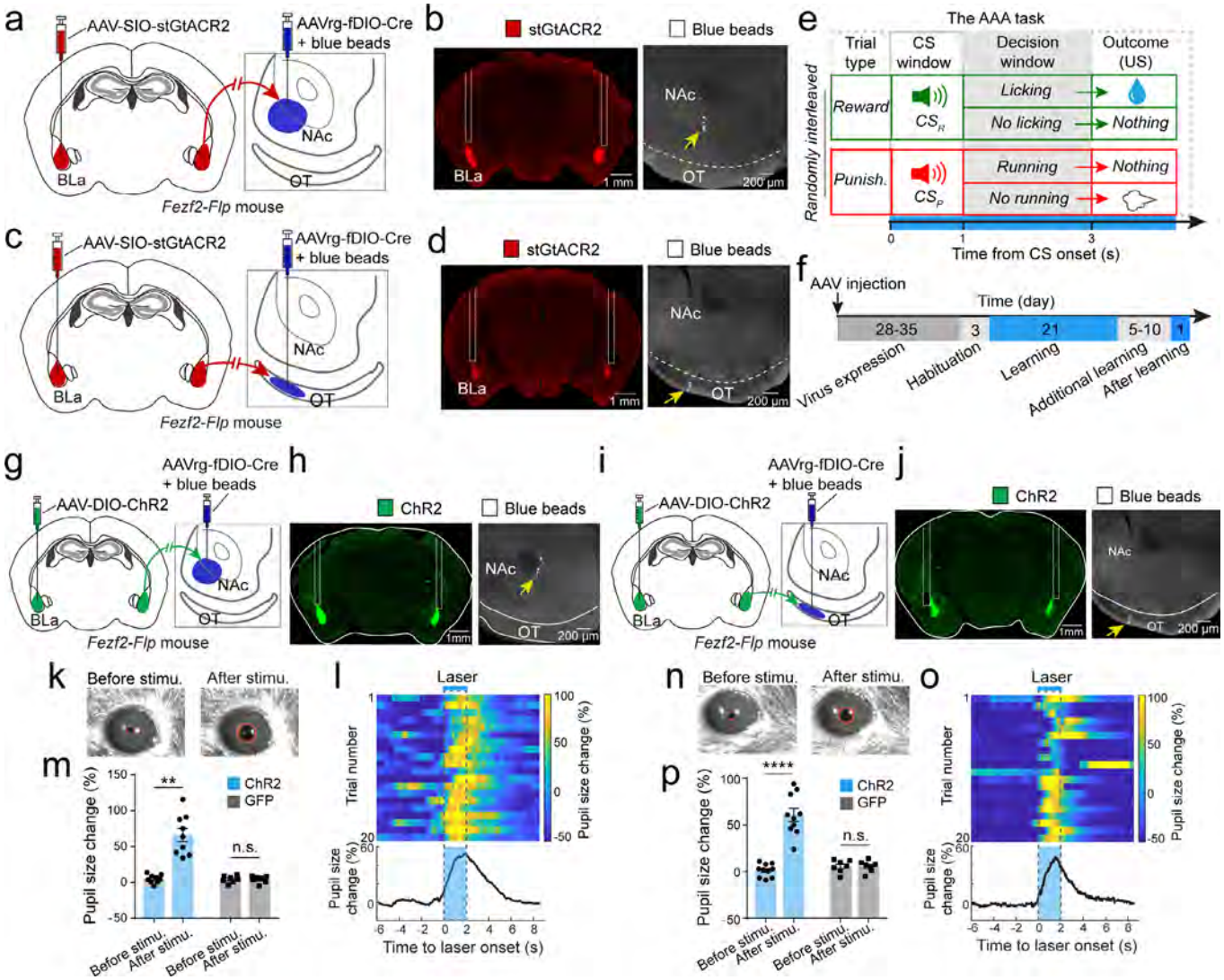

Extended Data Fig. 9 | Optogenetic manipulation of Fezf2$^{BLa\rightarrow NAc}$ and Fezf2$^{BLa\rightarrow OT}$ neurons. a-f, Optogenetic inhibition of Fezf2$^{BLa\rightarrow NAc}$ and Fezf2$^{BLa\rightarrow OT}$ neurons. **a**, A schematic of the approach to selectively inhibit Fezf2$^{BLa\rightarrow NAc}$ neurons with optogenetics. **b**, Left: a confocal image showing Fezf2$^{BLa\rightarrow NAc}$ neurons expressing stGtACR2. Locations of optical fibers for optogenetics are indicated. Right: a confocal image showing injection location of AAVrg-fDIO-Cre in the NAc, as indicated by fluorescent beads (arrow). **c**, A schematic of the approach to selectively inhibit Fezf2$^{BLa\rightarrow OT}$ neurons with optogenetics. **d**, Left: a confocal image showing Fezf2$^{BLa\rightarrow OT}$ neurons expressing stGtACR2. Locations of optical fibers for optogenetics are indicated. Right: a confocal image showing injection location of AAVrg-fDIO-Cre in the OT, as indicated by fluorescent beads (arrow). **e, f**, Schematics of the AAA task (e; blue bar on time axis indicates laser delivery) and experimental procedure (f). **g-p**, Optogenetic activation of Fezf2$^{BLa\rightarrow NAc}$ and Fezf2$^{BLa\rightarrow OT}$ neurons increases pupil size. **g**, A schematic of the approach to selectively activate Fezf2$^{BLa\rightarrow NAc}$ neurons with optogenetics. **h**, Left: a confocal image showing Fezf2$^{BLa\rightarrow NAc}$ neurons expressing ChR2. Locations of optical fibers for optogenetics are indicated. Right: a confocal image showing injection location of AAVrg-fDIO-Cre in the NAc, as indicated by fluorescent beads (arrow). **i**, A schematic of the approach to selectively activate Fezf2$^{BLa\rightarrow OT}$ neurons with optogenetics. **j**, Left: a confocal image showing Fezf2$^{BLa\rightarrow OT}$ neurons expressing ChR2. Locations of optical fibers for optogenetics are indicated. Right: confocal image showing injection location of AAVrg-fDIO-Cre in the OT, as indicated by fluorescent beads (arrow). **k**, Images of the pupil in a representative mouse, before (left) and after (right) photoactivation of Fezf2$^{BLa\rightarrow NAc}$ neurons. **l**, Trial-by-trial pupil size changes in response to photoactivation (blue bar, 2 s) of Fezf2$^{BLa\rightarrow NAc}$ neurons in an example mouse. **m**, Quantification of pupil size change in response to laser stimulation in the BLa in all the mice in which ChR2 (n = 9) or GFP (n = 7) was expressed in Fezf2$^{BLa\rightarrow NAc}$ neurons (Kruskal-Wallis test (K-stat 18.88) with Dunn's post-hoc test: $P = 0.0003$; ChR2: $^{**}P = 0.002$; GFP: $P = 0.99$). **n, o**, same as (k, l), respectively, except that Fezf2$^{BLa\rightarrow OT}$ neurons were photoactivated. **p**, Quantification of pupil size change in response to laser stimulation in the BLa in all the mice in which ChR2 (n = 10) or GFP (n = 7) was expressed in Fezf2$^{BLa\rightarrow OT}$ neurons (Kruskal-Wallis test (K-stat 21.9) with Dunn's post-hoc test: $P < 0.0001$; ChR2: $^{****}P < 0.0001$; GFP: $P = 0.99$).

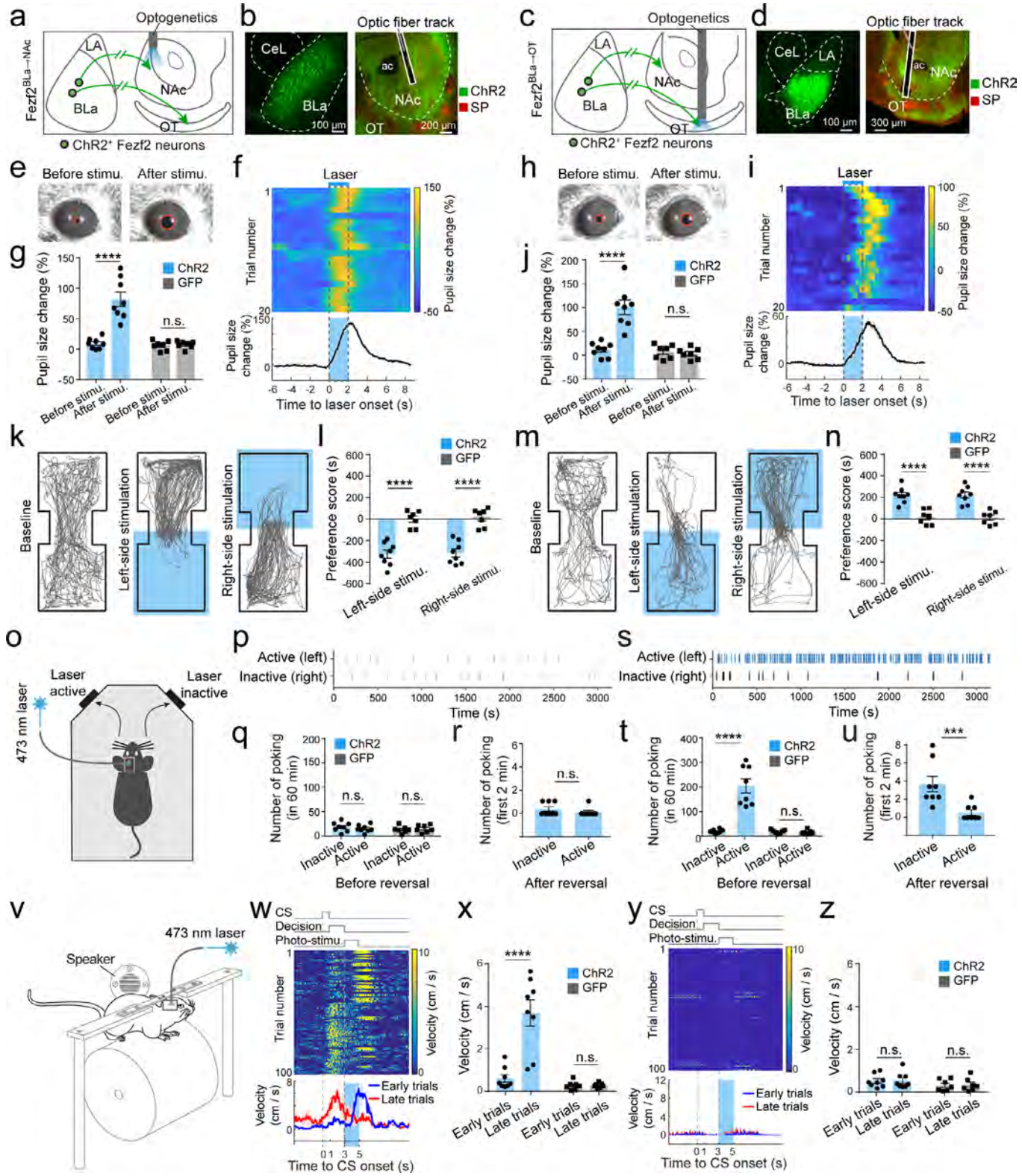

Extended Data Fig. 10 | See next page for caption.

Extended Data Fig. 10 | Fezf2$^{BLa\rightarrow NAc}$ and Fezf2$^{BLa\rightarrow OT}$ projections differentially instruct valence-specific learning. a, A schematic of the approach to stimulate the Fezf2$^{BLa\rightarrow NAc}$ pathway. **b**, Confocal images of the BLa (left) and ventral striatum (right) from a representative mouse, showing Fezf2^{BLa} neurons expressing ChR2 and ChR2^{+} axon fibers originating from Fezf2^{BLa} neurons, respectively. The placement of optical fiber in the NAc is also shown. Antibodies recognizing SP were used to label the ventral pallidum, which lies in between the NAc and OT. **c, d**, Same as a, b, respectively, except that the Fezf2$^{BLa\rightarrow OT}$ pathway was the target for optogenetic stimulation (c), and the optical fiber was placed over the OT (d). **e**, Images of the pupil in a representative mouse, before (left) and after (right) photoactivation of the Fezf2$^{BLa\rightarrow NAc}$ pathway. **f**, Trial-by-trial pupil size changes in response to photoactivation (blue bar, 2 s) of the Fezf2$^{BLa\rightarrow NAc}$ pathway in an example mouse. **g**, Quantification of pupil size change in response to laser stimulation in the NAc in all the mice in which ChR2 (n = 8) or GFP (n = 7) was expressed in Fezf2$^{BLa\rightarrow NAc}$ neurons ($F(1, 26) = 32.52$, $P < 0.0001$; $^{****}P < 0.0001$, n.s., $P = 0.9999$; two-way ANOVA followed by Bonferroni's multiple comparisons test). **h, i**, same as e, f, respectively, except that the Fezf2$^{BLa\rightarrow OT}$ pathway was photoactivated. **j**, Quantification of pupil size change in response to laser stimulation in the OT in all the mice in which ChR2 (n = 8) or GFP (n = 7) was expressed in Fezf2$^{BLa\rightarrow OT}$ neurons ($F(1, 26) = 30.34$, $P < 0.0001$; $^{***}P < 0.0001$, n.s., $P = 0.9999$; two-way ANOVA followed by Bonferroni's multiple comparisons test). **k**, Movement trajectory of a representative mouse at baseline (left), or in a situation whereby entering the left (middle) or right (right) side of the chamber triggered photoactivation of the Fezf2$^{BLa\rightarrow NAc}$ pathway. **l**, Quantification of mouse activity as shown in (k), for mice in which ChR2 (n = 8) or GFP (n = 7) was expressed in Fezf2^{BLa} neurons. The ChR2 mice, but not the GFP mice, avoided the side associated with the photo-stimulation ($F(1, 26) = 89.75$, $P < 0.0001$; $^{****}P < 0.0001$, n.s., $P > 0.05$; two-way ANOVA followed by Bonferroni's multiple comparisons test). **m, n**, Same as k, l, respectively, except that the Fezf2$^{BLa\rightarrow OT}$ pathway was targeted. The ChR2 mice (n = 8), but not the GFP mice (n = 7), preferred the side associated with the photo-stimulation ($F(1, 26) = 63.28$, $P < 0.0001$; $^{****}P < 0.0001$, n.s., $P > 0.05$; two-way ANOVA followed by Bonferroni's multiple comparisons test). **o**, A schematic of the approach. **p**, Raster plot of nose-poking events at active or inactive port, for a mouse in which ChR2 was expressed in Fezf2^{BLa} neurons and photo-stimulation was delivered to the NAc at the active port. **q**, Quantification of nose-poking events in a 60-min session for mice in which ChR2 (n = 8) or GFP (n = 7) was expressed in Fezf2^{BLa} neurons and photo-stimulation was delivered to the NAc at the active port ($F(1, 26) = 1.4$, $P = 0.25$; n.s., $P > 0.05$; two-way ANOVA). **r**, Quantification of nose-poke events of the ChR2 mice in q, in the first 2 mins of the reversal test, in which the active and inactive ports were switched ($P = 0.57$; Mann-Whitney test, $U = 24$). **s**, Same as p, except that photo-stimulation was delivered to the OT at the active port. **t**, Same as q, except that the Fezf2$^{BLa\rightarrow OT}$ pathway was targeted. The ChR2 mice (n = 8), but not the GFP mice (n = 7), vigorously poked the active port ($F(1, 26) = 35.43$, $P < 0.0001$; $^{***}P < 0.0001$, n.s., $P > 0.05$; two-way ANOVA followed by Bonferroni's multiple comparisons test). **u**, Quantification of nose-poke events of the ChR2 mice in t, in the first 2 mins of the reversal test, in which the active and inactive ports were switched ($^{***}P = 0.0003$; Mann-Whitney test, $U = 0.5$). **v**, A schematic of the approach. **w**, Top: trial-by-trial heat-maps of running velocity for an example mouse in the active avoidance task; bottom: average running velocity of the mouse in early (first 10 trials) and late (last 10 trials) trials. **x**, Quantification of running velocity during the decision window in early (first 10) and late (last 10) trials (ChR2 mice, n = 8, GFP mice, n = 7; ($F(1, 26) = 29.66$, $P < 0.0001$; $^{****}P < 0.0001$, n.s., $P > 0.05$; two-way ANOVA followed by Bonferroni's multiple comparisons test). **y, z**, Same as w, x, respectively, except that the Fezf2$^{BLa\rightarrow OT}$ pathway was targeted (ChR2 mice, n = 8, GFP mice, n = 7; ($F(1, 26) = 2.976$, $P = 0.096$; n.s., $P > 0.05$; two-way ANOVA followed by Bonferroni's multiple comparisons test). Data are presented as mean ± s.e.m.

nature research

Corresponding author(s): Bo Li

Last updated by author(s): Aug 12, 2021

Reporting Summary

Nature Research wishes to improve the reproducibility of the work that we publish. This form provides structure for consistency and transparency in reporting. For further information on Nature Research policies, see our Editorial Policies and the Editorial Policy Checklist.

Statistics

For all statistical analyses, confirm that the following items are present in the figure legend, table legend, main text, or Methods section.

n/a	Confirmed
☐	☒ The exact sample size (*n*) for each experimental group/condition, given as a discrete number and unit of measurement
☐	☒ A statement on whether measurements were taken from distinct samples or whether the same sample was measured repeatedly
☐	☒ The statistical test(s) used AND whether they are one- or two-sided *Only common tests should be described solely by name; describe more complex techniques in the Methods section.*
☒	☐ A description of all covariates tested
☐	☒ A description of any assumptions or corrections, such as tests of normality and adjustment for multiple comparisons
☐	☒ A full description of the statistical parameters including central tendency (e.g. means) or other basic estimates (e.g. regression coefficient) AND variation (e.g. standard deviation) or associated estimates of uncertainty (e.g. confidence intervals)
☐	☒ For null hypothesis testing, the test statistic (e.g. *F*, *t*, *r*) with confidence intervals, effect sizes, degrees of freedom and *P* value noted *Give P values as exact values whenever suitable.*
☒	☐ For Bayesian analysis, information on the choice of priors and Markov chain Monte Carlo settings
☒	☐ For hierarchical and complex designs, identification of the appropriate level for tests and full reporting of outcomes
☒	☐ Estimates of effect sizes (e.g. Cohen's *d*, Pearson's *r*), indicating how they were calculated

Our web collection on statistics for biologists contains articles on many of the points above.

Software and code

Policy information about availability of computer code

Data collection	Behavioral data were collected with custom-written scripts in MATLAB (R2015b, The MathWorks, Inc., Natick, Massachusetts, USA). Pupil size data were collected by an infrared-filter mounted camera (FL3-U3-13S2C-CS, Point Grey) with an open source Bonsai software (Bonsai, version 2.3.1). In vivo imaging data were collected by a custom-built wide-filed one-photon fluorescence microscope with software written in LabView (LabView2014, version 14, National Instruments). Fiber photometry data was collected by a commercial fiber photometry system (Neurophotometrics Ltd) with Bonsai software (Bonsai, version 2.3.1). The RTPP behavior of the mice were videotaped with a CCD camera (C930, Logitech) interfaced with Ethovision software (XT11.5, Noldus Information Technologies, Wageningen, The Netherlands). Whole-cell patch clamp recording from NAc or OT neurons was obtained with Multiclamp 700B amplifiers and pCLAMP 10 software (version 10.2.0.12, Molecular Devices, Sunnyvale, California, USA)
Data analysis	Confocal data for histology were analyzed using ImageJ (V1.52k, NIH). For in vivo imaging data processing and analysis, we used Mosaic (version 1.0.0b; Inscopix, Palo Alto, CA) t) and the extended constrained non-negative matrix factorization (CNMF-E) software written in Matlab. Behavioral, fiber photometry and decoding data were analyzed with custom-written scripts in Matlab (2015b, 2018b and 2019b; Mathworks). Statistical analyses were performed and plotted with Matlab or Prism7 (GraphPad). Offline video analysis for pupil size was conducted using EthoVision XT software (XT11.5, Information Technologies; Wageningen, The Netherlands).

For manuscripts utilizing custom algorithms or software that are central to the research but not yet described in published literature, software must be made available to editors and reviewers. We strongly encourage code deposition in a community repository (e.g. GitHub). See the Nature Research guidelines for submitting code & software for further information.

Data

Policy information about availability of data

All manuscripts must include a data availability statement. This statement should provide the following information, where applicable:

- Accession codes, unique identifiers, or web links for publicly available datasets
- A list of figures that have associated raw data
- A description of any restrictions on data availability

All data are contained in the main text, extended data or supplementary data. Source data can be downloaded at https://figshare.com/articles/dataset/NN-A72265C/15130017. Source code can be downloaded at https://figshare.com/articles/software/code_for_NN-A72265C/15157614.

Field-specific reporting

Please select the one below that is the best fit for your research. If you are not sure, read the appropriate sections before making your selection.

☒ Life sciences ☐ Behavioural & social sciences ☐ Ecological, evolutionary & environmental sciences

For a reference copy of the document with all sections, see nature.com/documents/nr-reporting-summary-flat.pdf

Life sciences study design

All studies must disclose on these points even when the disclosure is negative.

Sample size	No statistical methods were used to pre-determine sample sizes but our sample sizes are similar to those reported in previous publications (Xiao, X., et al., 2020; Stephenson-Jones, M., et al., 2020; Zhang, X. & Li, 2018).
Data exclusions	An animal was excluded if the viral injection location (as indicated by a virally expressed fluorescent protein or co-injected blue beads) was outside of the target area, such as the BLa, NAc or OT. If the tip of an implanted GRIN lens or optical fiber was outside of the target area, or if the behavioral performance could not reach the pre-established threshold in the imaging and fiber photometry experiments, the mouse was also excluded. No other mice or data points were excluded.
Replication	To ensure that results are reproducible, we included detailed methods, sources of reagents and protocols for all the experiments. All behavioral experiments were successfully repeated with the indicated numbers of mice. Individual data points and error bars were presented in the figures. All imaging data were collected from the specified numbers of cells. All histological experiments were successfully repeated. Exact sample sizes are provided in the figure legends, extended data figure legends, or supplementary figure legends.
Randomization	All mice were randomly assigned to different groups.
Blinding	Data collection and analyses were not performed blind to the conditions of the experiments. However equal parameter and process were consistently applied for all groups. Behavioral experiments and analyses were performed by investigators with knowledge of the identity of the experimental groups. However, all behavioral experiments were controlled by computer systems, and data were collected and analyzed in an automated and unbiased way.

Reporting for specific materials, systems and methods

We require information from authors about some types of materials, experimental systems and methods used in many studies. Here, indicate whether each material, system or method listed is relevant to your study. If you are not sure if a list item applies to your research, read the appropriate section before selecting a response.

Materials & experimental systems

n/a	Involved in the study
☐	☒ Antibodies
☒	☐ Eukaryotic cell lines
☒	☐ Palaeontology and archaeology
☐	☒ Animals and other organisms
☒	☐ Human research participants
☒	☐ Clinical data
☒	☐ Dual use research of concern

Methods

n/a	Involved in the study
☒	☐ ChIP-seq
☒	☐ Flow cytometry
☒	☐ MRI-based neuroimaging

Antibodies

Antibodies used	The primary antibodies used in this study were: rabbit anti-CaMKII (1:500; Abcam, catalog number ab52476, lot number GR312537-6), rabbit anti-GABA (1:500; Sigma, St. Louis, MO, USA; catalog number A2052), chicken anti-GFP (1:1000; Aves Labs, Catalog number GFP1020, lot number GFP697986), rabbit anti-RFP (1:1000; Rockland, Catalog number 600-401-379, lot number

35868), rabbit anti-Substance P (1:1000; ImmunoStar, Catalog number 20064, lot number 1531001), rabbit anti-HA-Tag (1:1000; Cell Signaling, Catalog number 3724S), rabbit anti-mCherry (1:1000; Abcam, catalog number ab167453, lot number GR3213077-3) and rabbit anti-DARPP32 (1:1000; Abcam, Catalog number ab40801). The fluorophore-conjugated secondary antibodies used were Alexa Fluor® 488 donkey anti-chicken IgG (H+L) (1:1000; Catalog number 703-545-155, Jackson ImmunoResearch), Alexa Fluor® 488 goat anti-rabbit IgG (H+L) (1:1000; Catalog number A-11008, Invitrogen) and Alexa Fluor® 555 goat anti-rabbit IgG (H+L) (1:1000; Catalog number A-21428; Life Technologies, Carlsbad, California, USA).

Validation

All the primary antibodies were validated by extensive previous studies (e.g., Stephenson-Jones et al, 2016, Nature; Zhang and Li, 2018, Nature Communications; Stephenson-Jones et al, 2020, Neuron), and by the manufacturers.

Animals and other organisms

Policy information about studies involving animals; ARRIVE guidelines recommended for reporting animal research

Laboratory animals	Male and female mice with age of 2-4 months were used in all the experiments. The strains used were Fezf2-2A-CreER or Fezf2-2A-Flp knock-in mouse lines, Ai14 and H2B-GFP reporter lines. All mice were bred onto a C57BL/6J background.
Wild animals	The study did not involve wild animals.
Field-collected samples	The study did not involve samples collected from the field.
Ethics oversight	Institutional Animal Care and Use Committee of Cold Spring Harbor Laboratory.

Note that full information on the approval of the study protocol must also be provided in the manuscript.